The Hudson Volcano and surrounding monogenetic centres (Chilean Patagonia): An example of volcanism associated with ridge–trench collision environment

F. Gutiérrez[a], A. Gioncada[b], O. González Ferran[a,c], A. Lahsen[a], R. Mazzuoli[b,*]

[a]*Departamento de Geología, Univ. de Chile, Santiago de Chile, Chile*
[b]*Dipartimento di Scienze della Terra, Univ. di Pisa, via S. Maria 53, I-56126 Pisa, Italy*
[c]*Departamento de Geografia, Univ. de Chile, Santiago de Chile, Chile*

Abstract

Hudson Volcano (45°54′S, 72°58′W) represents the southernmost central volcano of the South Andean Volcanic Zone (SVZ). It lies about 280 km east of Nazca–Antarctic–South American Plate Triple Junction, where the Chile spreading ridge enters the Chile Trench. Hudson is located on the border of a volcanic gap separating the Southern from the Austral Volcanic Zone (AVZ), which is commonly interpreted as linked to a slab window. The volcano is characterised by a volcano-tectonic depression about 10 km wide, set in a morphological high of the Patagonian Batholith. The scarce pre-caldera products are made up of mafic lavas interbedded with hyaloclastite. The majority of the volcanic products out from the caldera rims consist of thick deposits of lahars or hyaloclastitic breccias, subordinate lava flows and pyroclastic deposits linked to historical large explosive eruptions. Rough volume calculations on pre-caldera and post-caldera products suggest that the caldera formed in steps in the lifetime of the volcano and that it is mainly linked to a volcano-tectonic collapse during partial emptying of the magma chamber. The monogenetic cones surrounding Hudson (Río Ibanez and Murta) erupted primitive basalts that gave important clues on magma sources. The volcanic products of Hudson, with composition ranging from basalts to dacites, have a calc-alkaline signature. Nevertheless, they have distinctly higher K_2O, TiO_2, Na_2O, LILE, HFSE and REE than the calc-alkaline rocks of SVZ. The basaltic lavas from the monogenetic cones show La/Nb, Ba/Nb and Th/Ta significantly lower than the calc-alkaline lavas. Furthermore, they have some ratios as Th/Yb and La/Yb remarkably low, with values approaching those of MORB-like basalts. All the geochemical characteristics of Río Ibanez and Murta cones are very similar to those of the basalts dredged in the Chile Ridge. Geochemical modeling suggests that the Hudson basalts may derive from the basalts erupted at the Río Ibanez centre through an assimilation plus fractional crystallisation process. On the basis of these data, we propose a geodynamical model. In correspondence to the monogenetic centres, close to the border of the incipient opening of the slab window, the magma features are still those of the depleted asthenosphere under the subducting ridge. In this zone, remnant fragments of subducted oceanic crust undergo partial melting processes, while the mantle wedge is deeply modified by subduction-related components. In correspondence to Hudson and the nearby monogenetic centres, the MORB-type primary source component is modified by

* Corresponding author. Fax: +39 050 2215800.
E-mail address: mazzuoli@dst.unipi.it (R. Mazzuoli).

altered oceanic crust and variably mixed with andesitic magmas having a calc-alkaline signature. A contribution from partial melting of the continental lithosphere may be present in the complex source mixing process at the border of the slab window.

Keywords: Hudson Volcano; Southern Patagonia; calc-alkaline magmas; ridge subduction; geochemistry

1. Introduction

The southernmost sector of the South Andean Volcanic Zone (SVZ) is characterised by the alignment of large composite central volcanoes (e.g., Macá, Cay and Hudson) and several monogenetic spatter and cinder cones associated with lava flows, aligned along the main tectonic structures. Hudson Volcano, located at 45°54′S and 72°58′W, is the southernmost central volcano of SVZ and is sited on the border of the volcanic gap. It lies about 280 km east of Nazca–Antarctic–South American Plate Triple Junction, where the Chile Rise, an active oceanic spreading ridge, enters the Chile Trench. The gap in the active volcanic arc separates this volcano and the surrounding monogenetic centres from the Austral Volcanic Zone (AVZ). The lack of recent volcanism occurs just east of where the Chile Rise has been recently subducted (Fig. 1; Forsythe and Nelson, 1985; Forsythe et al., 1986; Stern et al., 1990; Stern, 1991a). The volcanic gap has been interpreted as due to a slab window related to the collision of Chile Ridge with the South America Plate, which started in Miocene time in the southern sector of the South America margin and continued in time northward (Ramos and Kay, 1992; Gorring et al., 1997).

The volcanic products of the SVZ are typically calc-alkaline and are linked to the subduction of the Nazca Plate under the South America Plate. When plate subduction is linked to the formation of a slab window, the dynamics of magma generation must be particularly complex. In these zones, the primary magmas may derive from partial melting of the metasomatised mantle wedge above the subducting plate, possibly modified by sub-slab asthenospheric melts due to vertical mantle flow through the slab window, or from continental lithosphere and/or slab melts (Guivel et al., 1999; Lagabrielle et al., 2000; Gorring and Kay, 2001; D'Orazio et al., 2001). The complexity of the geochemical characteristics may be enhanced by contamination with crustal materials having different composition during the storage of magmas in the crust and during their ascent to the surface.

The slightly oblique convergence of the Nazca–Antarctic Plates and the South America continent produces complex geological features on the continental margin. In the southernmost SVZ, the geological structures are dominated by the transcurrent dextral Liquini Ofqui (LOF) fault system (Hervé, 1984), a very complex system made up of the intersection of lineaments with NNE–SSW, NE–SW and NNW–SSE strike (Fig. 1). The melt generation and ascent processes in this area are strongly controlled by these regional structures, which, in a general compressive frame, generate extensional stress linked to strike-slip movements (Cembrano et al., 1996a,b).

In recent times, several eruptions of Hudson have been recorded (Deruelle and Bourgois, 1993; Naranjo and Stern, 1998). Widespread fallout deposits of andesitic to dacitic composition emitted by this volcano are intercalated with paleosols in Chilean Patagonia. In the last 30 years, Hudson was active two times. A Plinian eruption and lahar in 1971 was followed in 1991 by a larger plinian eruption. The few chemical analyses from Hudson are mainly referred to distal pyroclastic deposits of eruptions occurred in the last 6 ka (Naranjo and Stern, 1998). In fact, the volcano is scarcely known because it is remote from human settlements and for the intense vegetation at its feet that make it practically inaccessible. The monogenetic centres surrounding the Hudson Volcano (HV) are mainly characterised by strombolian scoria and lapilli and thin lava flows.

In February 2002, a geological survey was carried out in the Hudson volcanic area, during which it was possible (with the help of helicopter) to create a geological sketch map, to collect rock types and to observe the main geological and volcanological structures. In this paper, geological and volcanological data together with major and trace element geochemical data of HV and the surrounding volcanic centres are presented with the aim: (1) to investigate

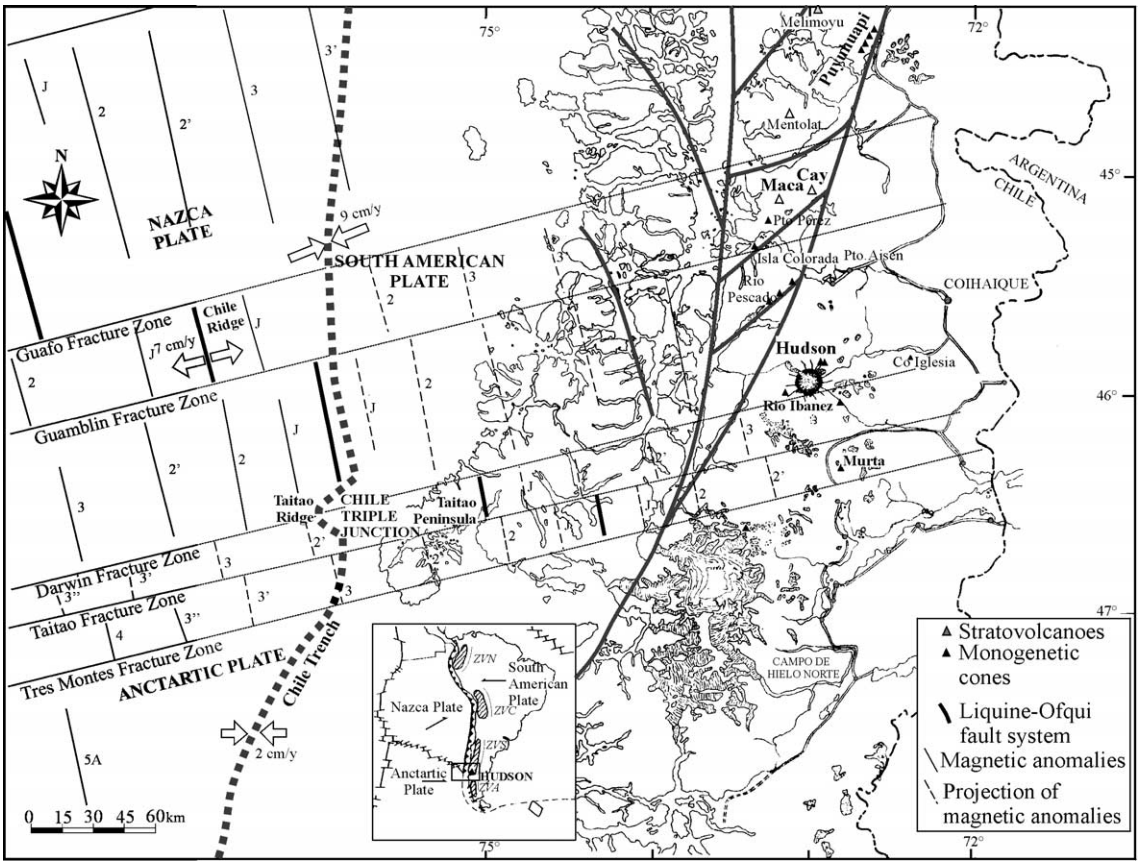

Fig. 1. Sketch map of the southernmost tip of the South Volcanic Zone, showing the relevant tectonic elements: the position of the Chilean spreading ridge, the margins of the Nazca and the Antarctic Plates, the Liquine–Ofqui fault system. The continuation of the structures under the continent showing the probable position of the subducting Chile Ridge, inferred on the basis of the spreading rate, is also reported (modified from Herron et al., 1981; Serv. Nac. Geol. Min., 1982; Naranjo et al., 1993; Nelson et al., 1994; Cembrano et al., 1996a,b).

the main structural and volcanological characters of a volcanic complex up to now very scarcely known; (2) to investigate the relationships between tectonics and volcanism in a geodynamically very complex area; and finally (3) to provide new geochemical data on a volcano at the border of a volcanic gap where a slab window is opening. These data could shed light on the petrogenetic processes acting in a geodynamic setting dominated by ridge–trench collision.

2. Geological and tectonic setting

The plate geometry of the area between 45° and 47°S in Chilean Patagonia is dominated by the interaction of Nazca and Antarctic Plates that are subducting under the South America continent. The Chile Ridge system collided with the South America continental margin about 14 Ma ago. At present, the ridge is colliding in correspondence of the Chile Triple Junction, just west of Taitao Peninsula (Fig. 1; Cande and Leslie, 1986, 1987). North of the Taitao Peninsula, the angle between the convergence vector of the Nazca Plate and a perpendicular to the strike of the Chile Trench is 22° and the convergence rate is 9 cm/year. South of the triple junction, the Antarctic Plate is converging at a rate of 2 cm/year and with a convergence angle of 0–2°. For this reason, the triple junction is migrating northward (Herron et al., 1981; Cande and Leslie, 1986, 1987; Fig. 1). South of the triple junction the recent orogenic volcanism as well as the seismic activity

is lacking down to 49°S. South of 49°S, adakitic magmas are erupted along the AVZ. These are produced by partial melting of the subducted young oceanic crust of the Antarctic Plate (Stern and Kilian, 1996). The gap zone, between 46.5° and 49°S, is interpreted to correspond to the slab window, which allowed the asthenospheric mantle to rise and give origin to the intraplate magmatism, developed in the South Patagonian back-arc (Ramos and Kay, 1992; Gorring et al., 1997; Gorring and Kay, 2001; D'Orazio et al., 2001). The southernmost sector of the active volcanic arc of SVZ is formed by Maca and Cay (MC hereafter) and the HV central composite volcanoes and surrounding monogenetic centres (Stern et al., 1990; Lopez-Escobar et al., 1993; D'Orazio et al., 2003). Volcanic products with adakitic composition, basalts with MORB characteristics and felsic intrusive bodies (all <4 Ma) are present in Taitao Peninsula (Fig. 1; Guivel et al., 1999; Lagabrielle et al., 2000).

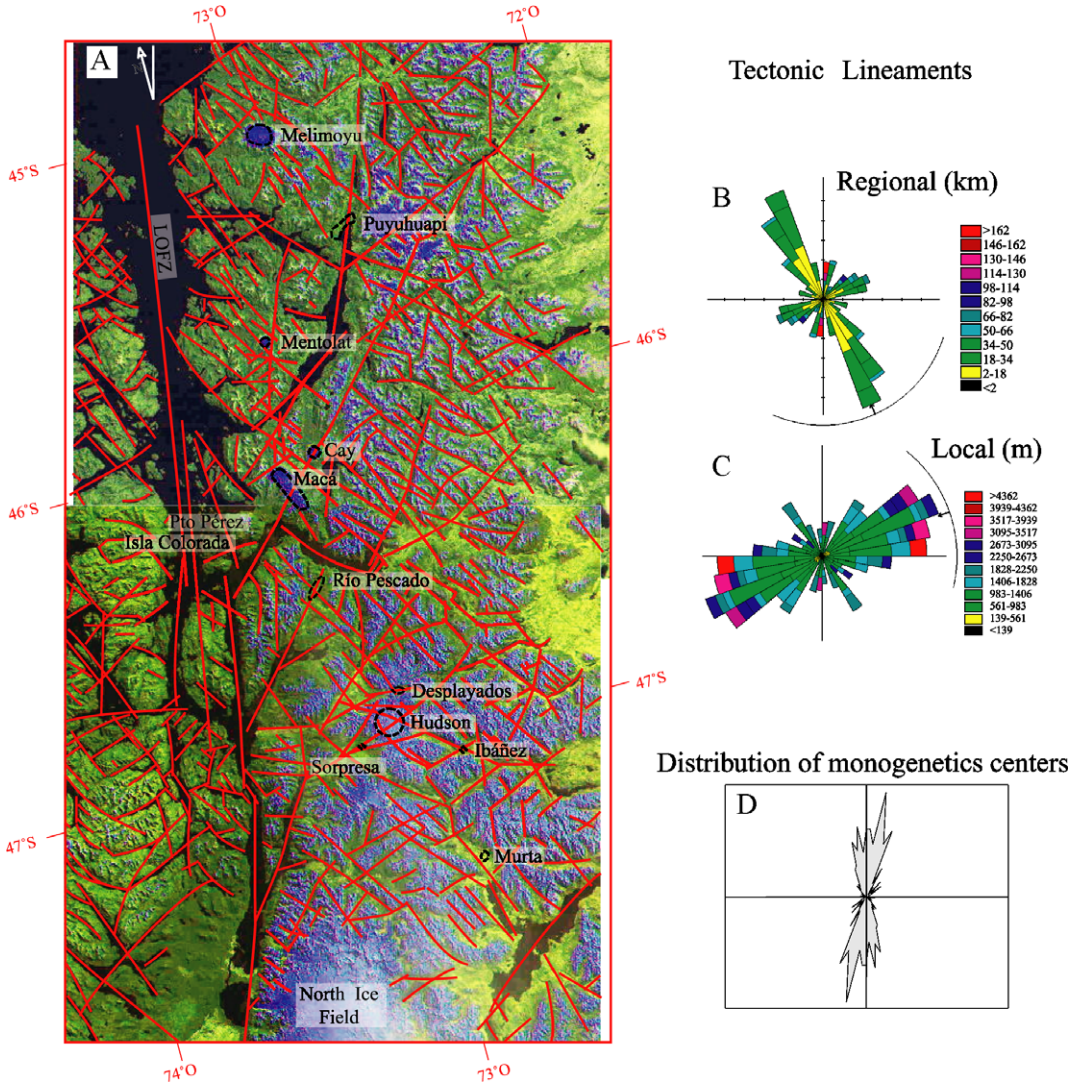

Fig. 2. (A) Main tectonic lineaments of the southernmost SVZ, reported on a Landsat image. (B) Rose diagram of the main tectonic lineaments on a regional scale. (C) Rose diagram of the main tectonic lineaments on a local scale, in correspondence of the Hudson Volcano. (D) Results of Fry analysis, applied to the distribution of the monogenetic cones in the area of (A).

Along the SVZ, the distribution of the volcanic centres is strongly related to tectonics and in particular to the LOF system. This system (Figs. 1 and 2A), linked to the oblique convergence of the Nazca–Antarctic Plates, is constituted by two main dextral transcurrent faults with NNE–SSW strike and at least 1000 km of length, joined by a series (at least four in the study area) en echelon lineaments with NE–SW strike and 10–30 km of length. Numerous lineaments with NNW–SSE strike also occur (Cembrano et al., 1996a,b). During the field survey, several fault direction measurements were collected that, together with observations of satellite images, permitted to construct the rose diagrams of Fig. 2B and C. The figure highlights that the regional tectonics is dominated by structures with NW–SE trend, parallel to the direction of the spreading ridge (Fig. 2B), whereas the NE–SW tectonics is the most developed in a local frame around the Hudson Volcano (Fig. 2C). The most extensive, though the less numerous, faults (>160 km) are those related to the NNE–SSW trending LOF system (Fig. 2B). Fig. 2D shows the distribution of the monogenetic centres carried out with Fry analysis (Vearncombe and Vearncombe, 1999), which indicates that the centres are roughly aligned along the NNE–SSW strike, that is along the LOF system trend.

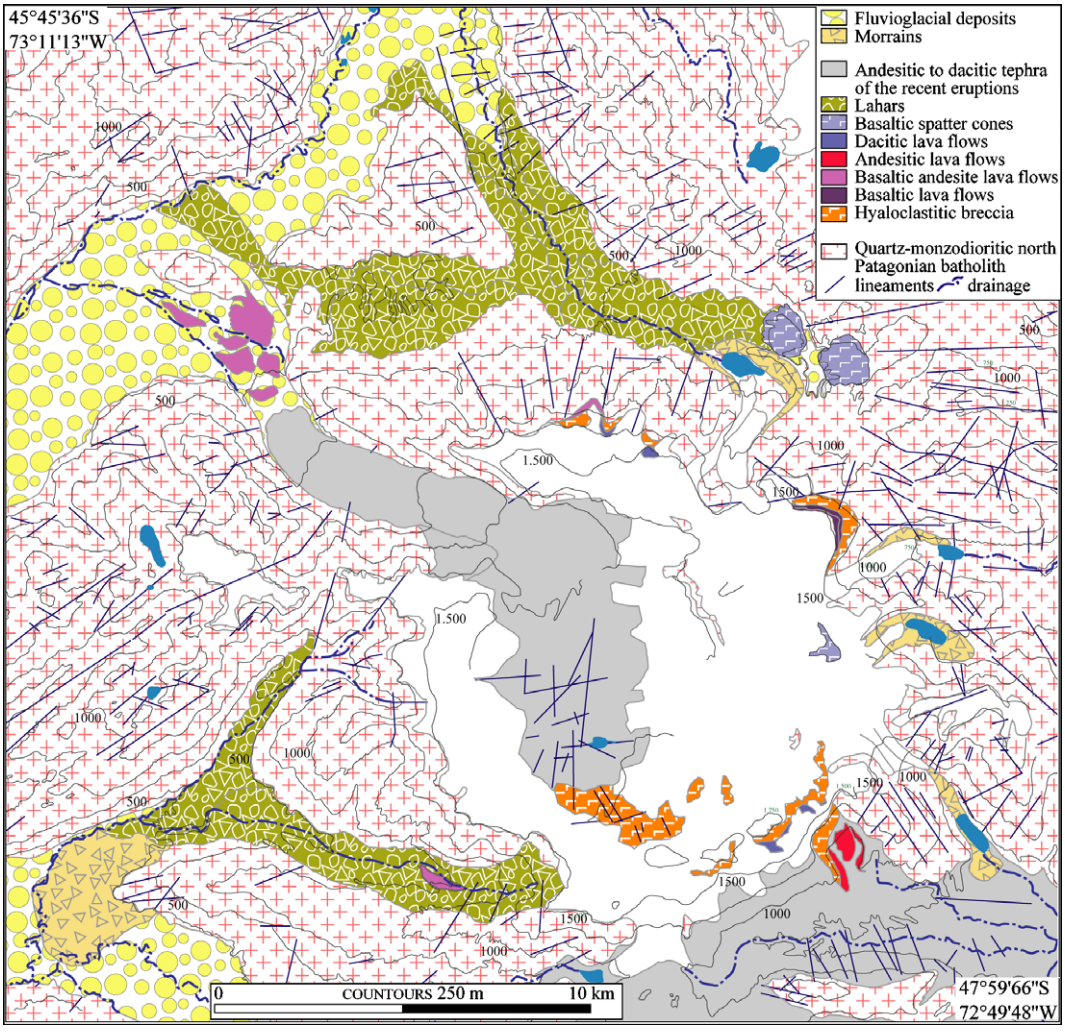

Fig. 3. Geological sketch map of the Hudson Volcano. The white pattern indicates ice cover.

Due to the particular geological conditions, the area between 45° and 49°S underwent intense vertical movements during the Miocene–Quaternary time. In the last 10 Ma, the average uplift/erosion rate has been calculated 1 mm/year and 3 mm/year (Hervé et al., 1993). Relevant changes in elevation on the order of meters have been recorded after some strong earthquakes (i.e., 1960 Chilean earthquake, Barrientos and Plafker, 1992).

The main geological unit of the region is represented by the Patagonian Batholith, a Cretaceous to Neogene (late Miocene) intrusive complex of about 1000 km in length that extends from latitude 41°S to 52°S. The geological data indicate an east–west zonation of the batholith: in the easternmost sector, the intrusive body shows a quasi-homogeneous leucomonzonite composition, whereas westwards it has diorite-tonalite and granodiorite composition (Pankhrust et al., 1994). Radiometric age determinations of the batholith decrease from west to east. The Hudson Volcano and its products are directly placed on the eastern Patagonian Batholith.

3. The Hudson Volcano

In Fig. 3, the geological sketch map of the Hudson Volcano is reported. The volcano is characterised by a volcano-tectonic depression about 10 km wide, set in a morphological high of the Patagonian Batholith, having a circular ("pancake") shape. The rims of the depression are mostly made up of the monzodioritic intrusive rocks of the batholith and only in the northeastern and southern external flanks of the depression do thick, pre-caldera volcanic sequences outcrop. Pre-caldera sequences are mainly constituted by mafic lavas (some with typical polygonal cooling fractures), hyaloclastitic breccias, lahars and pyroclastic deposits. The depression is filled by ice. In the northwestern sector of the depression a glacier, covered by the 1991 dark tephra, flows out of the caldera rim and forms the headwaters to the Huemules River (Branney and Gilbert, 1996). The tephra cover indicates that the glacier is flowing in a valley just below the permanent ice limit and during the austral summer it is snow free. Thus, the glacier,

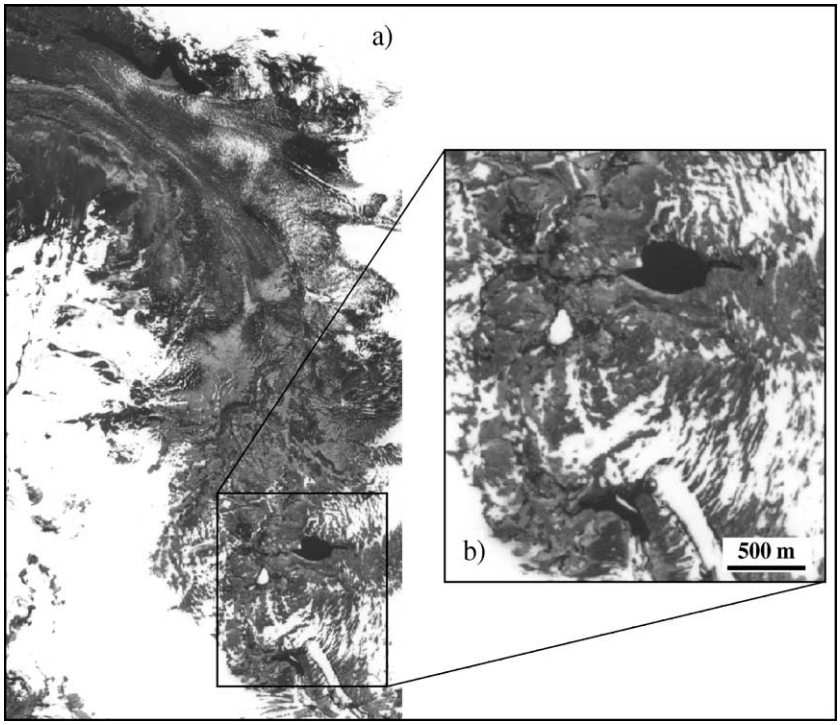

Fig. 4. The Rio Huemules glacier, flowing NW out of the Hudson caldera rim (aerial photo GEOTECSAF 1993 F101873). A small crater lake is visible inside the Hudson caldera, probably linked to the 1991 eruption.

when observed in the summer from a helicopter or in aerial photos, looks like a lava flow (Fig. 4). At the head of the glacier, a vent, presently occupied by a small lake, is well observable. This vent was probably active during the last eruption in 1991.

The majority of the volcanic products outside of the caldera rims are represented by thick deposits of lahars, subordinate lava flows and pyroclastic deposits linked to large explosive eruptions. The pyroclastic deposits are also found at large distances from the caldera (Stern, 1991b; Naranjo and Stern, 1998). The lahars are usually constituted by abundant fine grained matrix and poligenic clasts of altered, generally mafic lavas and minor intrusive blocks up to 1–2 m in diameter. Hyaloclastitic breccias are found at the rim of the caldera reaching a thickness of 150 m. The post-caldera lava flows are scarce and mainly occur as thin flows in the Huemules and Sorpresa Sur valleys. In this latter sector, the most recent lavas are associated with small spatter cones. The southern sector of the map area is characterised by the presence of thick layers of pyroclastic products linked to the most recent subplinian or plinian explosive eruptions. These are constituted by fall deposits of usually banded pumice clasts with scarce lithic fragments. The monogenetic spatter and cinder cones nearby HV show morphological features indicating they are very recent, coeval with HV products. They reach a maximum height of 200/300 m and are characterised by low volumes of basaltic

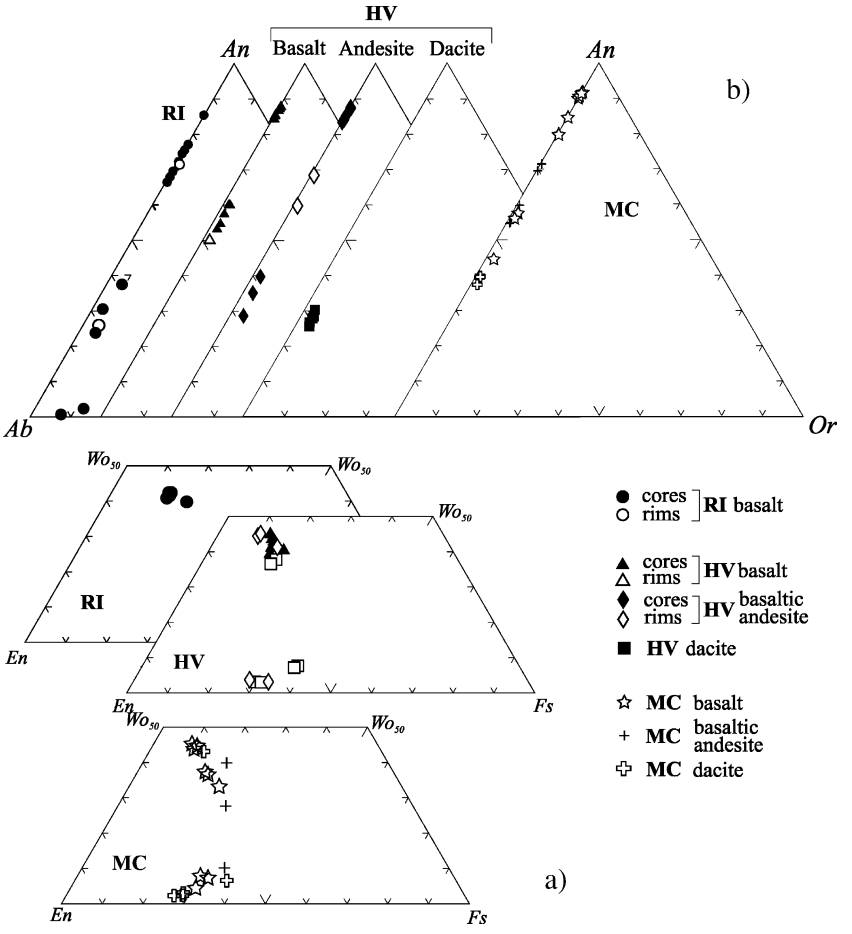

Fig. 5. (a) Composition of pyroxene in a Wo–En–Fs diagram (a) and of plagioclase plotted in an Ab–An–Or diagram (b) from samples of Río Ibanez, Hudson, Maca and Cay volcanoes. See legend for symbols.

Table 1
Representative analyses of the main mineral phases occurring in the products of Hudson, Río Ibanez, Maca and Cay Volcanoes

Mineral sample provenance	Plagioclase									
	HV123		HV18		HV6		HV65		HV28	
	RI		HV		HV		MC		MC	
	Core	Rim	Core	Rim	Core	Rim	Core	Rim	Core	Rim
SiO_2 (wt.%)	49.61	50.82	46.96	54.76	62.52	61.35	46.51	49.11	58.3	58.52
Al_2O_3	32.21	32.3	33.97	27.33	24.22	24.4	35.74	33.64	26.91	27.02
FeO	0.35	0.64	0.37	0.88	0.45	0.3	0.55	0.8	0.44	0.54
CaO	15.49	14.56	17.33	10.22	5.37	5.98	18.59	16.09	8.45	8.36
Na_2O	2.52	3.11	1.64	5.48	8.28	8.02	0.91	2.23	6.96	7.02
K_2O	0.03	0.15	0.04	0.3	0.63	0.59	0.04	0.06	0.18	0.2
Sum	100.21	101.58	100.31	98.97	101.47	100.64	102.34	101.93	101.24	101.66
An	77.12	71.49	85.18	49.87	25.45	28.21	91.65	79.67	39.75	39.25
Ab	22.70	27.63	14.59	48.39	71	68.47	8.12	19.98	59.24	59.64
Or	0.18	0.88	0.23	1.74	3.55	3.31	0.23	0.35	1.01	1.12

Mineral sample provenance	Clino- and orthopyroxene											
	HV123		HV137		HV6		HV6		HV65		HV28	
	RI		HV		HV		MC		MC		MC	
	Core	Rim	Core	Rim	Core	Rim	Core	Rim	Core	Rim	Core	Rim
SiO_2 (wt.%)	51.18	51.46	51.82	50.70	53.98	54.97	50.77	52.24	50.87	53.78	54.43	54.94
TiO_2	0.87	0.91	0.61	0.81	0.27	0.34	1.05	0.37	0.64	0.33	0.28	0.40
Al_2O_3	2.47	2.74	2.73	3.28	0.42	0.64	2.72	0.17	5.81	0.89	0.92	0.71
FeO	9.16	9.33	6.27	6.39	20.03	19.29	9.62	22.51	6.53	19.53	18.78	18.15
MnO	0.18	0.20	0.12	0.18	1.67	1.50	0.66	1.89	0.15	0.49	1.15	1.23
MgO	15.30	15.33	16.15	15.57	23.44	24.43	15.51	18.69	15.71	22.53	25.58	27.40
CaO	20.22	21.08	21.85	21.87	1.50	1.56	18.93	3.38	20.97	3.95	1.24	1.23
Na_2O	0.36	0.44	0.31	0.41	0.08	0.06	0.50	0.12	0.31	0.05	b.d.l.	b.d.l.
K_2O	b.d.l.	0.02	b.d.l.	b.d.l.	b.d.l.	b.d.l.	b.d.l.	b.d.l.	b.d.l.	b.d.l.	b.d.l.	0.01
Cr_2O_3	b.d.l.	b.d.l.	0.03	0.34	b.d.l.	b.d.l.	0.01	0.06	0.34	0.03	b.d.l.	0.05
Sum	99.7	101.5	99.9	99.2	101.4	102.8	99.8	99.4	101.0	101.6	102.4	104.1
Wo	41.55	42.42	44.39	45.07	3.01	3.08	39.42	7.20	43.75	7.81	2.41	2.30
En	43.75	42.93	45.66	44.65	65.56	67.17	44.94	55.39	45.61	62.03	69.13	71.24
Fs	14.69	14.65	9.94	10.28	31.42	29.75	15.64	37.42	10.63	30.16	28.47	26.47

Mineral sample provenance	Fe–Ti oxides										Cr, Al-spinel	
	HV18	HV123	HV137	HV6	HV65	HV28	HV28	HV28	HV6	HV6	HV137	
	HV	RI	HV	HV	MC	MC	MC	MC	HV	HV	HV	
SiO_2	0.18	0.05	0.11	0.14	0.13	0.07	0.00	0.17	0.07	0.01	0.05	0.09
TiO_2	21.84	15.99	16.64	16.47	17.44	16.31	45.63	46.19	48.63	48.52	2.28	1.79
Al_2O_3	0.51	3.29	2.39	1.95	1.81	1.89	0.23	0.26	0.17	0.12	18.93	23.36
FeO	71.07	75.39	74.86	76.68	75.27	76.12	49.03	47.98	46.36	46.72	37.51	34.73
MnO	0.76	0.58	0.87	1.17	0.29	1.67	1.17	1.08	1.47	1.46	0.28	0.19
MgO	0.59	3.21	2.78	2.1	2.1	1	2.91	2.83	3.03	3.00	10.91	11.47
CaO	0.2	b.d.l.	0.1	b.d.l.	b.d.l.	b.d.l.	b.d.l.	b.d.l.	b.d.l.	b.d.l.	0.15	0.2
Cr_2O_3	b.d.l.	b.d.l.	b.d.l.	b.d.l.	0.2	b.d.l.	b.d.l.	b.d.l.	b.d.l.	0.1	26.98	26.29
Sum	95.2	98.5	97.7	98.5	97.3	97.1	99.0	98.5	99.7	99.9	97.1	98.1
mol% Usp	63.5	43.0	45.6	45.2	48.5	45.6						
mol% Ilm							91.3	92.6	94.5	94.2		

andesitic to andesitic scoria and lapilli. Río Ibanez (RI hereafter) spatter cone, located 10 km southeast of HV, has been sampled and studied in detail here.

The most striking feature of the Hudson Volcano is the presence of a caldera 10 km wide set on the Patagonian Batholith. In fact, large parts of the exposed rims of the depression are constituted by monzodioritic rocks, while thick mafic lavas outcrop in some sectors of the rim. We presume that the formation of the HV relief may be favoured by a local upwelling due to the presence of a crystallising magma chamber. Considering the depression as a cylinder of 300 m high and a radius of 5 km, its volume is at least 23 km^3, but may be higher. A rough calculation of the products affected by the caldera faults and the hyaloclastites out of the caldera rim, based on our stratigraphic data, gave a volume of at least 6–8 km^3. The volume of tephra linked to the largest of the recent explosive eruptions, firstly retained responsible of the caldera formation (Stern, 1991a,b), is about 18 km^3 (6700 BP, Naranjo and Stern, 1998). It is noteworthy that the volume of magma erupted in a single event, even if the largest, is much lower than the minimum caldera volume, suggesting that the depression formed incrementally. Recent geological and geochronological data confirm that the present Hudson caldera formed by multiple collapse events (Orihashi et al., 2004). Tectonic movements possibly played a role in the caldera formation. Glacial erosion may be an additional factor affecting geomorphology at Hudson. The low volumes of pre-caldera volcanics and high volumes of the Holocene pyroclastic deposits may suggest that most of the caldera formation occurred in relatively recent times.

4. Petrography and mineral chemistry

Petrography and mineral chemistry revealed that magma mixing processes are very common in the HV shallow magmatic system, suggesting that scarcely differentiated basaltic magmas recurrently arrived in a shallow magma chamber and mixed with the resident, differentiated magmas.

Table 2
Composition of the glass and mineral phases forming the partially melted xenoliths in the Río Ibanez basalt

Phase	Glass	Albite	Sphene
Sample	HV123	HV123	HV123
	[2]	[2]	[2]
SiO_2 (wt.%)	75.58	68.14	30.07
TiO_2	0.75		34.43
Al_2O_3	11.05	20.46	2.56
FeO	2.71	0.06	1.77
MnO	0.04		0.07
MgO	0.40		0.02
CaO	0.20	0.31	27.29
Na_2O	3.58	9.93	0.04
K_2O	3.91	1.63	0.05
Sum	98.19	100.51	96.28
An		1.51	
Ab		88.90	
Or		9.59	

See Table 1 for analytical details; for glass, a defocused beam was used, to minimise alkali loss under the beam.

The phenocryst content is generally low in HV and RI rocks. The mineral assemblage in mafic terms involves plagioclase, olivine, clinopyroxene and Fe–Ti oxides. Two populations of plagioclase phenocrysts with contrasting composition characterise the HV basalts, ranging from $An_{88–84}$ to $An_{61–50}$ (Fig. 5a and Table 1). In the HV basalts, olivine and clinopyroxene phenocrysts also occur (Fig. 5b), but these are in equilibrium with a magma more evolved than a basalt (as indicated by the comparison of Fe/Mg of liquidus in equilibrium calculated according to Sisson and Grove, 1993). Therefore, the HV basalts can be the product of a mixing process between a rather primitive magma, testified by the presence of bytownite, and a slightly more evolved one, represented by labradorite, clinopyroxene and olivine. An-poor rims mantle An-rich cores and the groundmass has homogeneous texture, indicating that the physico-chemical properties of the mixing magmas permitted the achievement of chemical hybridisation.

Notes to Table 1:
Major and minor element analyses were performed on polished rock sections at CNR-IGG Firenze, using a JEOL JXA-8600 electron microprobe equipped with four WDS spectrometers integrated with an EDS system. Accelerating voltage and beam current were 15 kV and 10 nA, respectively, with variable counting times. When analysing feldspars, a defocused beam was used, to minimise alkali loss under the beam. The data were corrected using the Bence and Albee (1968) method. Standard deviation was lower than 3% for most major elements and 5% for minor ones (Vaggelli et al., 1999).

Several disequilibrium features characterise also the RI basalt. The main plagioclase population (Fig. 5a) having composition $An_{77–66}$ coexists with rounded and corroded crystals with composition $An_{37–24}$. Moreover, millimeter and submillimeter crystal aggregates composed of quartz, albite, sphene and a clear glass of acidic composition are dispersed in the basaltic rock (Table 2). This evidence suggests a process of melting and partial assimilation of rocks encountered during the rise of the basaltic magma to the surface.

In the most evolved rocks, orthopyroxene is abundant as a phenocryst phase, together with andesine-oligoclase (Table 1). Low-Ca clinopyroxene occurs as rims mantling both olivine and clinopyroxene crystals, indicating that these crystals were inherited and are not in equilibrium in the differentiated magmas. Fe–Ti oxides and apatite are common accessory minerals in the differentiated products. In HV high-K dacite and andesite, a magmatic Fe-sulfide occurs as inclusions in orthopyroxene and Ti-magnetite phenocrysts. Coexisting magnetite and ilmenite pairs occurring as phenocrysts in the HV and MC dacites were analysed. Their composition indicated temperatures averaging 760 °C for HV and 810 °C for MC, with oxygen fugacity averaging respectively ΔFMQ+2 and ΔFMQ+1.6 log units (Table 3).

The HV rocks with intermediate composition (andesite) are characterised by macroscopic and microscopic evidence of magma mixing in the form of bands of glass with contrasting colour of groundmass glass (transparent/brown) and texture (glassy/microlitic). The bands display distinct mineral assemblages. The clear glassy bands contains phenocrysts of plagioclase $An_{20–40}$, orthopyroxene, Ti-magnetite, ilmenite and apatite, while the microlitic groundmass corresponds to a magma having phenocrysts of plagioclase $An_{83–87}$, clinopyroxene with Mg-value up to 82 (Table 1) and a Cr-rich spinel (Table 1). This latter paragenesis corresponds to the most primitive basaltic magma erupted at Hudson Volcano.

Table 3
Temperature and fO_2 calculated from the composition of coexisting magnetite and ilmenite using the Spencer and Lindsley (1981) Fe–Ti oxide geothermometer

Sample	Rock	Provenance	$-\log fO_2$	T (°C)
HV6	dacite	Hudson	12.5	847
			14.6	728
			14.7	733
			14.2	746
MC28	dacite	Maca	14.2	764
			13.1	820
			12.5	852
			13.1	810
HV137	andesite with mingling	Hudson	13.7	791
			13.1	818
			13.2	813

Each temperature derives from a distinct mineral pair.

5. Geochemistry

The analysed samples of HV, RI and MC volcanic products are plotted in the TAS diagram (Fig. 6a). For comparison, in this and in the following diagrams, we plotted a field for the calc-alkaline SVZ and added data from the literature relative to monogenetic volcanic centres of the southernmost tip of SVZ: the Murta Volcano, which represents the southernmost centre before the volcanic gap (Demant et al., 1994), and the Puyuhuapi centres (González-Ferrán et al., 1996). The products of the Hudson Volcano range in composition from basalts and trachybasalts up to trachydacites (Table 4, Fig. 6a), with a gap in the SiO_2 ranging from 54 to 59 wt.%. The most primitive products belong to RI and plot on the HV trend. The RI and HV rocks straddle the curve of Irvine and Baragaar (1971) dividing the alkaline and subalkaline fields, while the MC rocks plot below that curve. Some basalts erupted by Puyuhuapi monogenetic cones fall in the alkaline field (Fig. 6a). The FeO/MgO ratios (not shown in the figure) indicate that the RI and HV rocks have a calc-alkaline character. In Fig. 6b, the most primitive rocks of RI and HV fall in the calc-alkaline field but with a K_2O wt.% content higher than the MC and in general the SVZ products. The most differentiated rocks plot instead in the high-K andesite and dacite fields (Fig. 6b).

Major and trace elements analyses of representative samples of the products of HV, RI and MC volcanoes are quoted in Table 4. In Fig. 7a,b, variation diagrams for selected major and trace elements are presented. The alkalis of the HV volcanics display positive trends with SiO_2, with contents significantly higher than the SVZ calc-

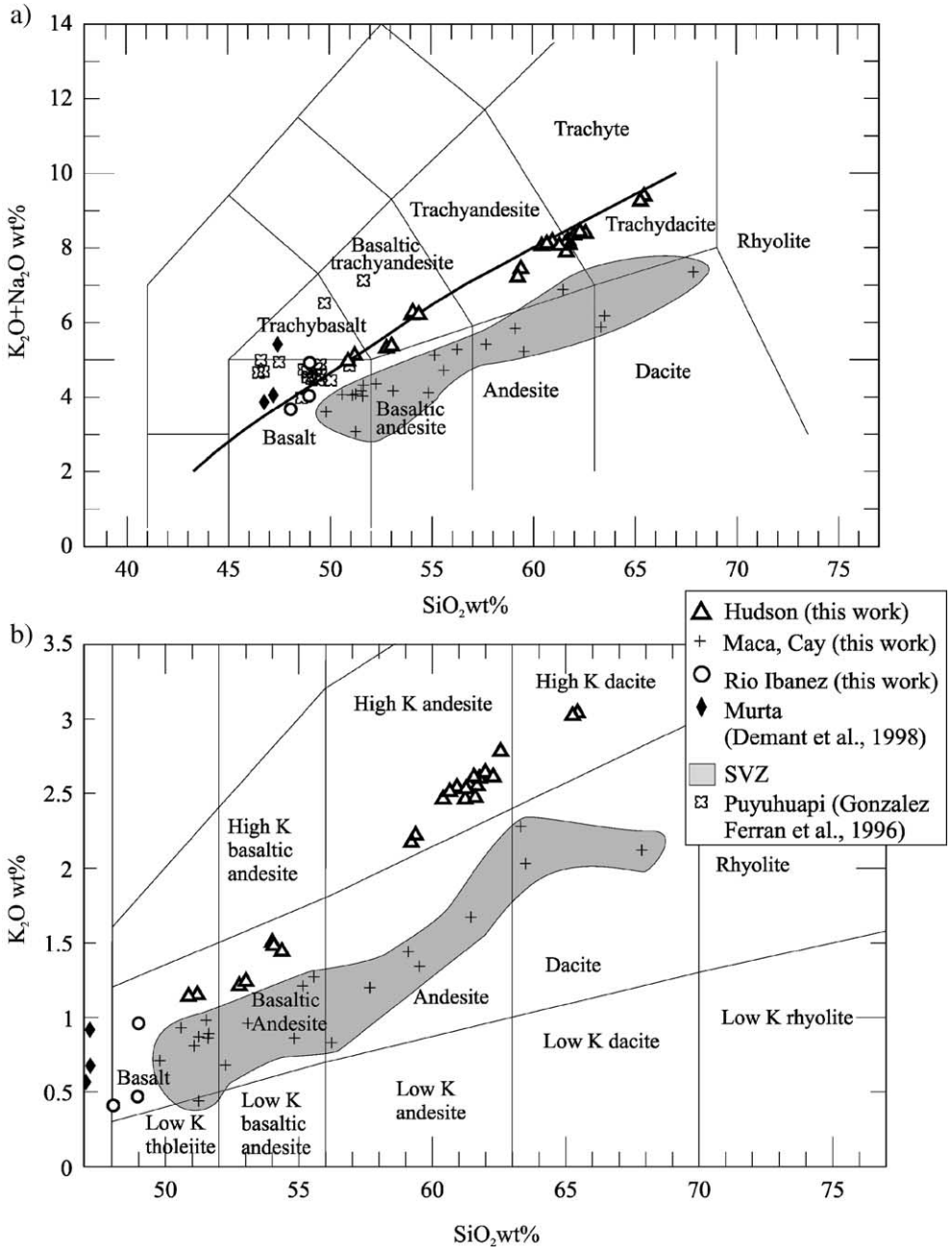

Fig. 6. (a) TAS (total alkali vs. silica) diagram showing the composition of the Hudson, Río Ibanez, Maca and Cay products (this work). Data from the literature are reported for comparison (Murta, from Demant et al., 1998; Puyuhuapi, González-Ferrán et al., 1996; calc-alkaline products of the South Volcanic Zone as a light grey field, Futa and Stern, 1988; Lahsen et al., 1997; D'Orazio et al., 2003). The field covered by the Maca and Cay samples nearly coincides with the variation of calc-alkaline SVZ volcanism. (b) K_2O vs. SiO_2 diagram of the Hudson, Río Ibanez, Maca and Cay products. Symbols and data sources as in (a).

Table 4
Representative analyses of samples from Hudson, Río Ibanez, Maca and Cay volcanic products

Sample	3	5	6	18	21	22	91	92	93	95	96
Provenance	HV	HV	HV	HV	HV	HV	HV	HV	HV	HV	HV
Longitude W	72°57′47″	72°57′47″	72°57′47″	72°53′42″	72°53′42″	72°53′42″	72°53′35″	72°53′35″	72°53′35″	72°53′35″	72°53′35″
Latitude S	45°51′42″	45°51′42″	45°51′42″	45°52′26″	45°52′26″	45°52′26″	45°57′35″	45°57′35″	45°57′35″	45°57′35″	45°57′35″
SiO_2 (wt.%)	52.76	61.68	65.44	51.20	59.37	50.86	65.25	62.56	61.77	61.56	61.99
TiO_2	2.01	1.35	0.94	1.78	1.59	1.76	1.02	1.35	1.45	1.45	1.40
Al_2O_3	16.62	16.07	15.98	16.90	16.08	16.83	16.05	15.93	16.03	16.09	16.03
FeO	7.00	3.92	3.76	7.70	4.60	7.59	2.67	4.03	4.21	3.36	4.21
Fe_2O_3	2.91	1.89	0.66	2.62	2.53	2.50	1.52	1.65	1.65	2.49	1.58
MnO	0.17	0.16	0.16	0.17	0.18	0.17	0.15	0.15	0.16	0.15	0.16
MgO	4.17	1.76	0.91	4.34	2.31	4.35	1.01	1.56	1.81	1.76	1.75
CaO	8.09	3.53	1.85	8.67	4.55	8.75	2.07	3.24	3.66	3.64	3.50
Na_2O	4.09	5.64	6.34	3.96	5.21	3.81	6.22	5.60	5.47	5.49	5.69
K_2O	1.21	2.55	3.04	1.15	2.22	1.14	3.02	2.78	2.60	2.61	2.64
P_2O_5	0.70	0.40	0.20	0.42	0.61	0.41	0.21	0.38	0.44	0.45	0.39
LOI	0.29	0.74	0.38	0.97	0.78	1.09	0.42	0.66	0.44	0.45	0.31
Mg-values	59	51	41	59	53	60	46	49	52	52	51
FeO_t/MgO	2.30	3.18	4.78	2.31	2.97	2.26	3.98	3.52	3.14	3.17	3.20
Be (ppm)	2.1		4.9	1.6	2.1			4	2.9		
Sc	30		13	33	18			18	16		
V	278	73	21	341	103	334	23	78	82	86	72
Cr	54	3	4	151	143	104	42	306	182	116	73
Co	25	11	2	31	8	34	7	6	7	12	10
Ni	18	3	3	16	3	13	2	9	4	3	3
Cu	49		10	53	11			15	13		
Rb	22	65	75	23.4	59	29	81	68	64	68	72
Sr	561	350	203	528	401	541	229	294	330	337	325
Y	34	51	58	30.4	42	30	55	52	50	51	51
Zr	222	478	508	162	273	180	528	422	386	430	447
Nb	12	20	23	9.6	15.1	10	23	18.8	18	19	19
Cs	0.34		2.07	0.66	1.93			0.91	1.96		
Ba	395	763	869	321	557	212	830	741	705	726	738
La	28.9	45	51	20	33	33	48	45	43	45	45
Ce	67	103	112	46	73	0	104	100	96	93	93
Pr	8.7		13.9	6.1	9.6			12.7	12.1		
Nd	36		54	26.3	40			50	50		
Sm	7.6		10.7	5.9	8.8			10.1	10.3		
Eu	2.18		2.65	1.75	2.31			2.55	2.51		
Gd	7.2		9.4	5.8	7.9			9.1	8.8		
Tb	1.09		1.59	0.89	1.28			1.47	1.48		
Dy	6.4		9.5	5.4	7.3			8.9	8.4		
Ho	1.29		2.04	1.09	1.46			1.86	1.71		
Er	3.5		5.9	3.1	4.1			5.2	4.9		
Tm	0.51		0.93	0.43	0.63			0.8	0.76		
Yb	2.98		5.9	2.69	4.1			5	4.9		
Lu	0.47		0.87	0.38	0.59			0.74	0.73		
Hf	5		11.7	3.7	6.6			9.4	8.9		
Ta	0.73		1.37	0.61	0.96			1.12	1.1		
Pb	5.2		16.2	5.6	10.6			15.9	14		
Th	2.78		8.4	3.01	6.4			7.4	6.9		
U	0.68		1.97	0.72	1.61			1.83	1.75		

97a	97b	98a	98b	104	107	108	109	111	137	140	142	114	122
HV	HV	HV	HV	HV	HV	HV	HV	HV	HV	HV	HV	HV	RI
72°53′35″	72°53′35″	72°53′35″	72°53′35″	72°46′15″	73°05′39″	73°06′20″	73°05′48″	73°05′48″	73°01′52″	73°01′52″	–	72°45′16″	72°42′08″
45°57′35″	45°57′35″	45°57′35″	45°57′35″	46°01′27″	45°50′33″	45°50′42″	45°51′04″	45°51′04″	45°57′56″	45°57′56″	–	46°00′08″	46°02′47″
60.40	62.28	60.92	61.23	61.61	54.00	54.06	54.36	60.65	59.21	53.01	61.26	61.26	48.04
1.44	1.25	1.43	1.42	1.39	1.97	1.84	1.88	1.47	1.12	1.75	1.43	1.43	1.40
15.97	16.00	15.91	16.05	16.07	16.23	16.90	16.77	15.97	16.96	16.93	16.05	16.05	17.50
3.47	0.00	3.60	0.00	0.00	7.13	7.03	8.07	0.00	4.46	7.08	0.00	0.00	5.31
2.98	5.90	2.80	6.41	6.38	2.62	2.20	1.02	6.77	1.72	3.06	6.50	6.50	4.50
0.19	0.18	0.19	0.19	0.19	0.18	0.17	0.17	0.21	0.15	0.18	0.19	0.19	0.16
2.30	1.94	2.23	2.29	2.10	3.46	2.80	2.98	2.23	2.48	3.56	2.11	2.11	9.25
3.75	3.19	3.61	3.55	3.48	7.07	7.15	7.13	3.78	5.18	7.63	3.55	3.55	10.44
5.58	5.81	5.62	5.58	5.41	4.69	4.78	4.76	5.59	5.04	4.12	5.52	5.52	3.26
2.46	2.61	2.54	2.46	2.47	1.50	1.48	1.44	2.51	2.17	1.24	2.53	2.53	0.41
0.38	0.32	0.36	0.35	0.36	0.66	0.67	0.77	0.37	0.33	0.51	0.36	0.36	0.16
0.85	0.00	0.59	0.00	0.00	0.25	0.44	0.31	0.00	0.74	0.60	0.00	0.00	0.35
56	55	55	57	55	55	51	53	56	58	55	55	55	77
2.66	2.71	2.73	2.50	2.71	2.73	3.20	3.02	2.70	2.42	2.75	2.74	2.74	1.01
2.7					1.8								
16					26								
67	55	62	64	56	258	222	264	62	117	243	255	58	190
2	2	2	4	4	52	11	58	3	57	33	111	2	243
5	10	10	11	10	20	26	28	11	17	28	29	11	45
1	2	3	3	2	3	3	5	2	12	12	13	3	93
12					27								
59	68	67	66	65	33	36	32	68	59	33	32	67	12
369	343	378	369	374	504	497	489	384	420	512	511	385	408
50	51	53	51	48	40	40	38	52	42	35	35	50	26
353	421	407	398	380	228	245	230	405	376	251	249	398	147
17.3	20	19	19	17	10.4	10	9	19	14	9	9	18	3
1.65					0.95								
694	736	712	728	714	466	476	478	720	676	452	459	724	69
40	44	42	42	42	30.1	29	30	43	41	27	27	45	5
89	92	84	90	90	71	62	68	87	77	59	62	93	29
11.5					9.5								
47					40								
9.8					8.6								
2.89					2.71								
8.7					8.2								
1.45					1.23								
8.3					7.3								
1.67					1.55								
4.7					4								
0.71					0.59								
4.9					3.6								
0.65					0.55								
7.9					5.4								
1.12					0.66								
11.7					7								
6.2					3.7								
1.54					0.92								

(continued on next page)

Table 4 (*continued*)

Sample	123	128	28	29	36	38	41	84	86	87	61
Provenance	RI	RI	Macá, 10 Km. SE	Macá, 10 Km. SE	Macá, 10 Km. SE	Macá, 10 Km. SE	Macá, 10 Km. SE	Macá, 10 Km. SE	Macá, 10 Km. SE	Macá, 10 Km. SE	Macá, 14 Km. SE
Longitude W	72°42′08″	72°42′08″	73°04′38″	73°04′38″	73°04′38″	73°04′21″	73°04′21″	73°05′22″	73°05′22″	73°05′22″	73°02′47″
Latitude S	46°02′47″	46°02′47″	45°12′48″	45°12′48″	45°12′48″	45°12′36″	45°12′36″	45°13′10″	45°13′10″	45°13′10″	45°15′30″
SiO_2 (wt.%)	48.95	48.99	67.86	59.52	55.14	63.49	63.31	59.09	61.44	57.66	49.79
TiO_2	1.35	1.60	0.63	0.76	1.44	0.85	0.83	1.03	1.03	1.09	0.99
Al_2O_3	17.82	16.94	15.45	16.69	16.78	15.82	15.57	17.04	16.67	16.80	18.57
FeO	5.48	5.96	1.21	4.62	6.72	2.44	1.64	4.74	3.91	3.00	4.37
Fe_2O_3	4.01	3.83	2.21	1.92	2.55	2.43	3.14	1.89	1.64	4.46	4.47
MnO	0.15	0.18	0.10	0.10	0.16	0.10	0.09	0.13	0.13	0.14	0.15
MgO	7.71	6.54	1.29	3.81	3.39	2.47	2.54	2.42	1.81	3.33	5.45
CaO	10.16	8.78	2.52	6.25	7.28	4.02	4.02	6.00	4.74	6.43	9.88
Na_2O	3.56	3.95	5.23	3.88	3.91	4.14	3.59	4.39	5.21	4.21	2.89
K_2O	0.47	0.96	2.12	1.34	1.21	2.03	2.28	1.44	1.67	1.20	0.71
P_2O_5	0.20	0.36	0.19	0.19	0.28	0.32	0.28	0.28	0.37	0.29	0.20
LOI	0.30	1.36	0.75	0.63	0.86	1.63	2.55	0.78	0.62	0.83	1.25
Mg-values	74	70	58	67	56	64	66	56	53	62	69
FeO_t/MgO	1.17	1.43	2.46	1.66	2.65	1.86	1.75	2.66	2.97	2.09	1.53
Be (ppm)	1	1.4	2.3						1.6		
Sc	28	30	12						17		
V	176	167	26	150	304	67	63	143	97	194	224
Cr	153	235	80	91	103	135	29	72	24	64	110
Co	38	34	2	24	28	11	10	20	9	21	30
Ni	81	76	3	39	10	4	2	6	4	11	34
Cu	49	45	7						18		
Rb	9	14.8	57	31	34	54	66	40	42	30	19
Sr	388	408	284	403	412	367	367	416	375	467	1033
Y	25.8	33	66	25	33	37	37	32	36	30	21
Zr	124	183	247	141	157	229	229	171	181	157	114
Nb	3.6	8.2	8.3	4	5	10	10	4	5.4	4	3
Cs	0.24	0.32	7.72						2.95		
Ba	102		583	323	309	467	467	370	438	376	287
La	9	15.5	30.2	13	18	37	25	13	19.2	15	16
Ce	22.9	37	61	41	34	55	55	48	44	44	54
Pr	3.2	5.1	10.4						6.2		
Nd	14.7	22.7	44						26.4		
Sm	3.8	5.6	9.7						6.3		
Eu	1.47	2.39	1.98						1.63		
Gd	4.2	5.5	9.9						6.4		
Tb	0.72	0.95	1.62						1.01		
Dy	4.5	5.7	9.6						6		
Ho	0.99	1.15	2.07						1.33		
Er	2.74	3.2	5.6						3.7		
Tm	0.41	0.47	0.83						0.56		
Yb	2.5	3.02	5						3.5		
Lu	0.37	0.43	0.77						0.54		
Hf	2.81	3.7	6.5						5		
Ta	0.27	0.56	0.56						0.36		
Pb	2.5	2.6	15.4						12		
Th	0.99	1.64	5.9						4.7		
U	0.23	0.41	1.62						1.3		

63	69	65	73	78	47	50	51	52	81	83	90
Macá, 2 Km., NE	Macá, 2 Km., SW	Macá, 2 Km., SW	Cay	Cay	Cay	Cay	Cay	Cay	monogenetic cone	Macá, 10 Km. SE	Pto Perez
73°06′11″	73°09′17″	73°09′17″	72°59′41″	72°58′12″	72°59′30″	72°59′30″	72°59′30″	72°56′46″	73°03′02″	73°02′53″	73°14′17″
45°06′09″	45°07′33″	45°07′33″	45°03′02″	45°02′40″	45°04′49″	45°04′49″	45°04′49″	45°03′27″	45°06′56″	45°12′14″	45°12′17″
56.23	53.08	51.25	51.63	51.53	51.60	51.25	50.58	51.08	52.25	55.57	54.83
1.36	1.24	0.76	1.27	1.09	1.05	1.08	0.95	1.07	1.36	0.82	0.78
16.51	17.32	18.40	18.01	18.00	18.11	18.15	18.76	18.93	17.76	17.03	18.03
6.92	4.99	5.78	6.41	6.30	5.06	5.57	4.98	6.20	6.14	5.27	5.46
2.66	4.15	2.47	2.90	2.60	3.67	3.35	3.48	2.91	3.51	2.39	2.68
0.18	0.14	0.13	0.14	0.14	0.14	0.14	0.13	0.14	0.16	0.13	0.14
3.23	4.22	6.52	4.57	5.28	5.70	5.32	5.50	5.57	3.32	5.66	5.28
6.72	8.72	11.26	9.45	9.84	9.52	9.74	10.05	9.72	7.81	7.83	8.35
4.45	3.20	2.63	3.43	3.18	3.16	3.21	3.13	3.24	3.67	3.44	3.25
0.83	0.96	0.44	0.89	0.98	0.86	0.87	0.93	0.81	0.68	1.27	0.86
0.31	0.19	0.11	0.23	0.27	0.24	0.21	0.19	0.20	0.21	0.14	0.12
0.31	1.34	0.37	0.42	0.34	0.41	0.57	0.52	0.24	1.58	0.50	0.47
54	62	73	63	67	70	68	70	68	55	72	69
2.88	2.06	1.22	1.97	1.63	1.46	1.61	1.47	1.58	2.79	1.31	1.49
		0.5						0.8			0.8
		32						27			25
284	263	242	282	253	271	263	247	251	403	164	209
54	98	162	83	134	144	144	177	125	65	186	255
29	29	30	34	33	35	35	34	30	32	27	28
4	16	40	26	41	43	38	49	31	6	64	32
		58						61			44
19	28	9.9	16	16	17	18	22	10.5	19	42	23
453	544	419	625	644	626	638	630	638	490	405	429
28	27	15	23	19	19	21	18	18.9	26	20	15.7
108	125	44	119	103	104	105	104	79	102	126	69
3	4	1.26	4	2	1	2	4	2.41	3	2	2.09
		0.69						0.32			1.52
233	243	129	252	267	241	238	253	228	190	303	225
16	11	4.6	14	11	9	14	17	9.4	8	11	7.3
41	49	11	50	48	44	58	37	22.9	42	25	16.4
		1.63						3.2			2.18
		7.8						14.9			9.4
		2.27						3.8			2.5
		0.78						1.26			0.99
		2.59						3.7			2.65
		0.42						0.57			0.45
		2.63						3.4			2.78
		0.57						0.71			0.59
		1.56						1.99			1.61
		0.23						0.28			0.25
		1.4						1.69			1.5
		0.22						0.27			0.22
		1.33						2.19			1.95
		0.09						0.16			0.17
		3.9						4.4			5.8
		0.82						1.63			2.2
		0.29						0.47			0.65

alkaline products, here represented by MC products. The MC basaltic rocks show higher Al_2O_3 contents than the HV and RI. TiO_2 increases from RI to HV basalts and then decreases regularly up to the most evolved rocks, with values higher than the MC products. P_2O_5 content shows a rapid increase up to samples with 56 wt.% of SiO_2, while between 60 and 65 wt.% of SiO_2 the values cluster at 0.4–0.2 wt.%. CaO and MgO are relatively lower than in the SVZ products. For a similar degree of differentiation, HV rocks show significantly higher contents in most of the incompatible elements and in the REE, compared to the rest of SVZ volcanics (Fig. 7b).

Chondrite-normalised REE patterns of the most mafic rocks of HV and RI are compared to the Murta, Puyuhuapi and SVZ basalts in Fig. 8a. The RI and Murta rocks show the same, almost flat REE pattern. The HV basalts are LREE-enriched and have a steeper negative slope than RI and Murta basalts. RI, Murta and HV rocks show higher REE contents than the calc-alkaline SVZ products. The REE patterns of the Puyuhuapi alkaline basalts have a markedly steeper negative slope. The REE values increase with the differentiation degree both in the HV (Fig. 8b) and MC (Fig. 8c) rocks. A slight negative Eu anomaly occurs only in the most evolved MC and HV dacites.

No primitive magma composition occurs in the HV samples. The basalts from the HV have Mg-values close to 50. Accordingly, their Ni and Cr contents are low (Fig. 7b). The most primitive rocks in this area are represented by the RI monogenetic cone products (Mg-value = 74–77, Table 1).

In the spiderdiagrams of rock composition normalised to primordial mantle (Fig. 9), only the samples with Mg-values higher than 66 are reported, together with the most primitive HV basalt. All the products show the Nb (and Ta, not shown) troughs characteristic of subduction-related magmatism, most evident in the SVZ rocks. The RI and Murta basalts shows a pattern strongly similar to Hudson, but with a lower content in all the elements on the left side of the diagram (Rb, Ba and Th but also Ta, Nb and LREE). The Puyuhuapi alkaline basalts lack or show a very limited Nb trough and have a general higher content in the most incompatible elements and a lower content in the elements Ti. . .Lu (Fig. 9).

6. Discussion

The geochemical data on the Quaternary volcanic products of the southernmost tip of SVZ indicate that magmas with strikingly different geochemical characters were erupted in few squared kilometers. The HV mafic rocks have geochemical characteristics at the transition from subalkaline to alkaline composition (Fig. 6a), whereas the basaltic andesites and andesites erupted by MC volcanoes show a typical calc-alkaline affinity similar to the majority of the SVZ volcanoes. The monogenetic volcanoes surrounding HV (i.e., RI and Murta) erupted quite primitive basalts with trace elements distribution markedly distinct in respect to the majority of the SVZ volcanoes (Fig. 9), with a particularly low abundance in Rb, Ba and Th. In the same sector of Andes, on the eastern branch of LOF at about 120 km north of Cay Volcano, some spatter cones (i.e., Puyuhuapi) erupted alkaline mafic magmas with peculiar trace element patterns, which lack the Nb–Ta troughs typical of the subduction-zone lavas and are more similar to within-plate magmas (González-Ferrán et al., 1996). The geological features of the monogenetic cones and the relatively primitive chemistry of their products suggest that magmas emitted by these centres erupted to the surface without ponding in

Notes to Table 4:
Mg-value = $Mg/(Mg+Fe^{2+})$, with $Fe^{3+}/Fe^{2+}=0.15$. Major and trace elements were analysed on powdered whole rock samples by XRF with a Philips PW 1480 instrument at Dip. Scienze della Terra, University of Pisa. The concentrations were calculated correcting for matrix effects following the method of Franzini et al. (1975). Accuracy was monitored using international standards and is better than 10% for concentrations higher than 10 ppm. The analyses of major oxides were compared by means of linear regression with those obtained by XRF on fused samples with an ARL 9400 XP þ instrumentation, carried out on about half of the samples, and corrections were applied when necessary. Fe^{2+} was obtained by titration. ICP-MS (VG PQII Plus) analysis (Dip. Scienze della Terra, Pisa) was carried out on a selection of samples, allowing the determination of a wide set of trace elements, with accuracy to within ±5%.

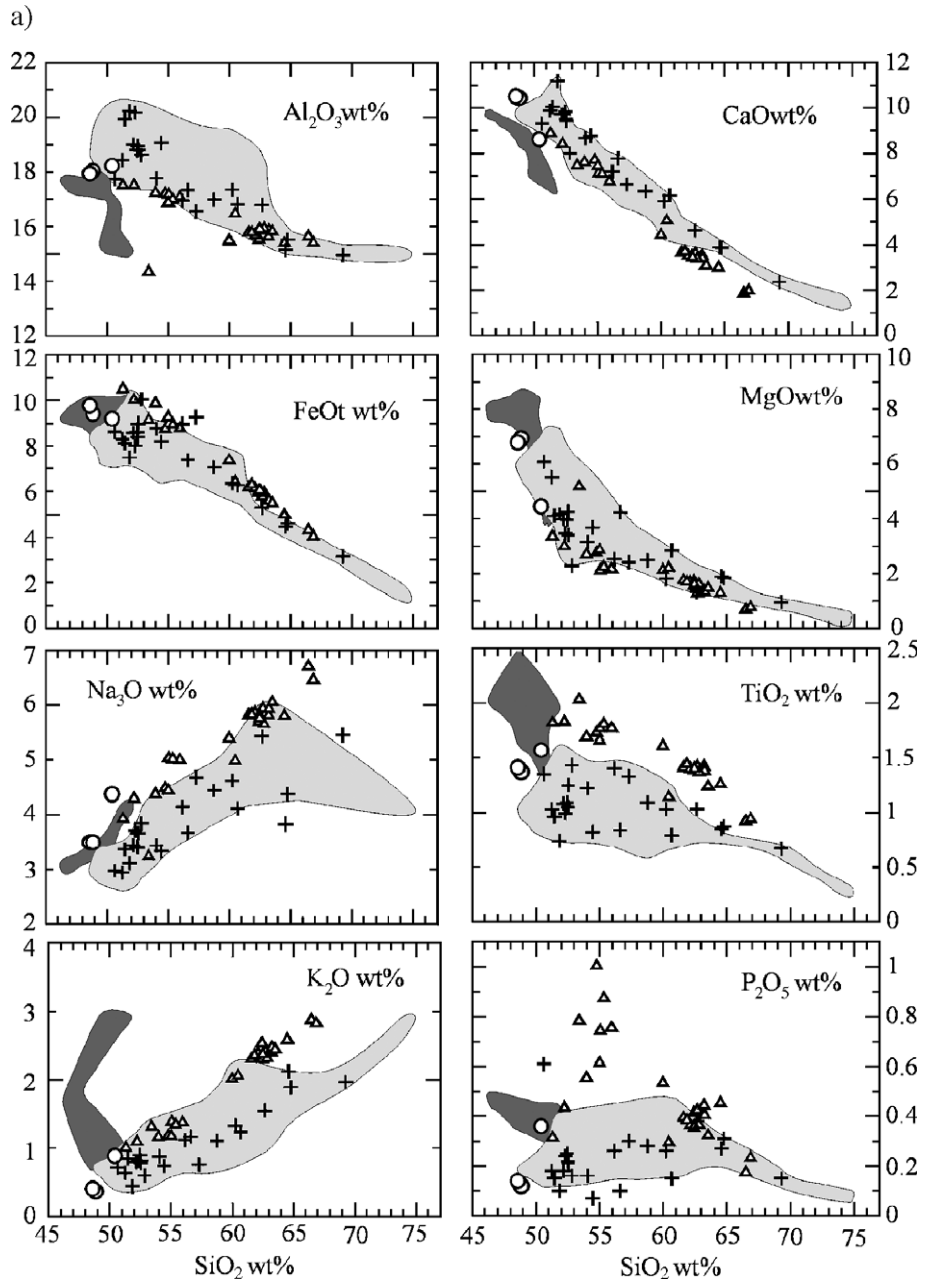

Fig. 7. Variation diagrams (a: major elements, b: trace elements) showing the composition of samples from Hudson, Río Ibanez, Maca and Cay (this work). Data from the literature are reported for comparison (light grey field: calc-alkaline products of the South Volcanic Zone; dark grey field: Puyuhuapi; symbols and data sources as in Fig. 6).

the crust. Thus, in order to define the magma sources, we must take into particular account the lavas linked to the monogenetic cones surrounding the HV. The characterisation of their magma sources allows us to discuss the chemical processes that affected the magmas, the tectonic regime in which the volcanism developed and its geodynamic significance.

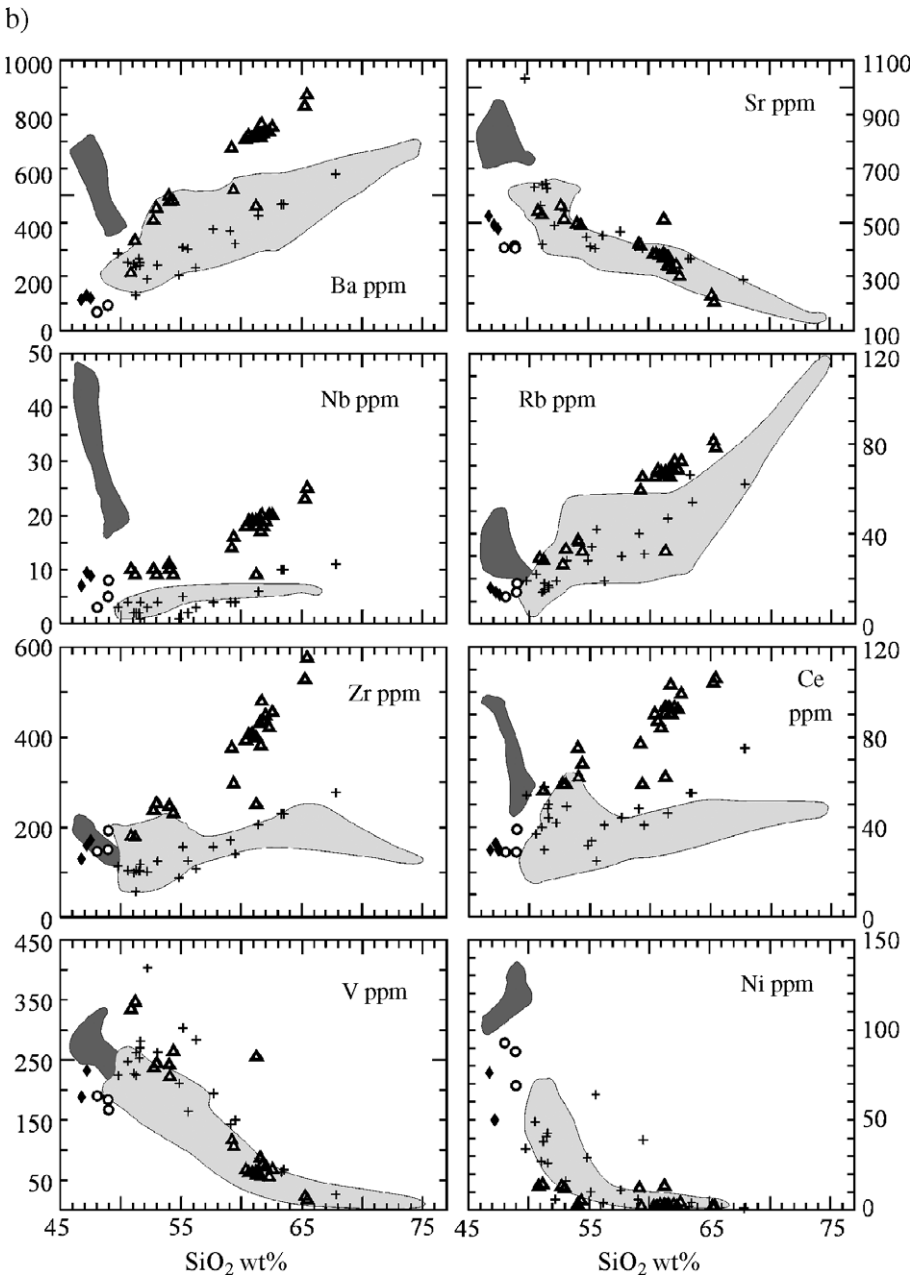

Fig. 7 (*continued*).

6.1. Magma sources

The trace element composition of the mafic rocks of RI, Murta and HV, the southernmost volcanoes of SVZ and the closest to the border of the slab window (Fig. 1), is shown in Fig. 10. In the diagram, trace element data from the Taitao Ridge, the SVZ and representative compositions of OIB and N-MORB are also plotted.

The HV basalt, having Mg-value = 55, shows trace element abundance higher than RI (Mg-value = 74–77)

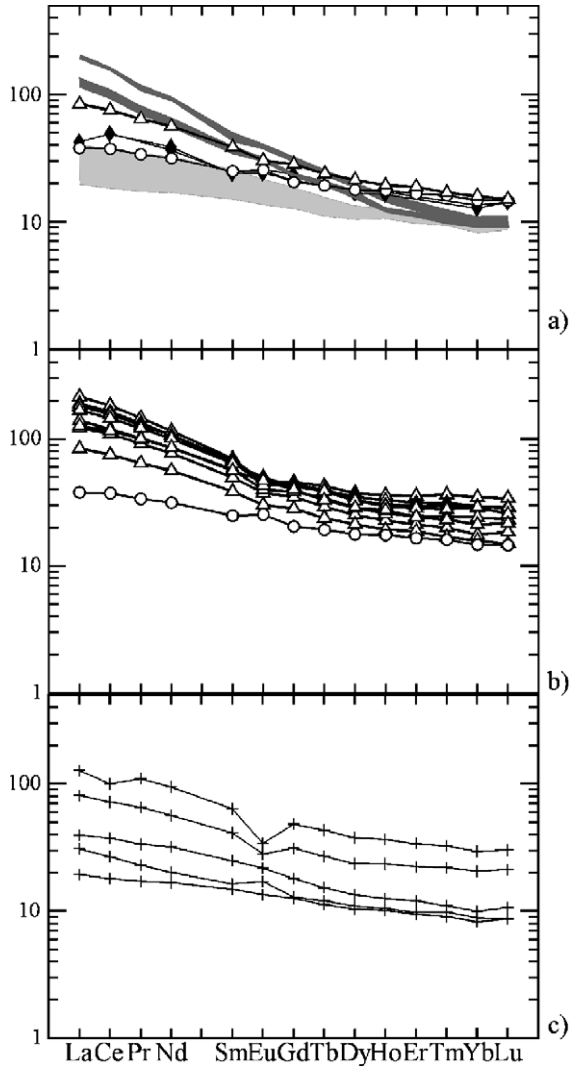

Fig. 8. (a) Chondrite-normalised REE patterns of the mafic rocks from Río Ibanez, Hudson, Maca and Cay (fields, symbols and data sources as in Figs. 6 and 7). (b) Chondrite-normalised REE patterns of the products of RI and HV volcanoes (this work), ranging in composition from basalt to high-K dacite. (c) Chondrite-normalised REE patterns of the products of Maca and Cay Volcanoes (this work), ranging in composition from basalt to dacite (normalisation factors from Sun and Mc Donough, 1995).

but with a remarkably similar pattern. This suggests that the trace element enrichment is mainly originated by differentiation processes. The RI and Murta basalts show lower abundance of the most incompatible elements (Cs, Ba, Rb and Th), a smaller negative Nb anomaly and markedly higher abundance of HFSE and other less incompatible elements (Zr...Yb), with respect to the SVZ calc-alkaline products. These characteristics are similar to some basalts sampled at the Taitao Ridge, the most relevant differences being that Taitao Ridge samples have lower abundance of Ba, LREE, Sr and P. Basalts from the Chile Ridge, sampled even farther from the continent, show similar patterns (Klein and Karsten, 1995). The peculiar composition of these Chile Ridge basalts was explained by contamination of sub-oceanic depleted mantle by marine sediments and altered oceanic crust, that could reach the sub-oceanic zone by a process of crustal recycling (Klein and Karsten, 1995; Guivel et al., 1999; Lagabrielle et al., 2000).

In Table 5, some incompatible trace element ratios that should be unaffected by early differentiation processes are reported. The RI, Murta and HV basalts show remarkably lower values of the LILE/HFSE ratios (i.e., Ba/Nb), and different ratios of mobile elements with contrasting affinity for a fluid or melt phase (i.e., Ba/La) with respect to the SVZ calc-alkaline rocks. La/Nb as well as Zr/Y trend to values observed in within-plate magmas, while the low Th/Yb approaches MORB composition. In the diagram $(La/Nb)_N$ vs. $(La/Yb)_N$ (Fig. 11a), discriminating the fields of N-MORB and E-MORB from the rocks with arc imprint, RI and Murta basalts, erupted along the volcanic arc, plot together with basalts of the Chile and Taitao Ridges (Klein and Karsten, 1995; Lagabrielle et al., 2000; Guivel et al., 1999). The rest of all products erupted in the area (MC, HV and Puyuhuapi) show very high values of these ratios and fall out of the field diagram (Fig. 11b). These features suggest that a modified MORB-type component similar to that occurring beneath the Chile Ridge, near the Chile Triple Junction, is involved in the source of RI and Murta basalts. This interpretation is strongly supported by the relatively depleted Sr isotope composition of Murta ($^{87}Sr/^{86}Sr$ 0.70359, Demant et al., 1998; Fig. 11d). However, other geochemical characters (i.e., Ba/Nb, Th/Ta, etc.) (Table 5 and Fig. 11c) suggest an arc component. The arc component may be acquired by the modified MORB type magmas interacting with pockets of fluid/melt modified mantle stored at the base of lithosphere. The high HFSE, Zr/Y and Ti/Y require an intraplate OIB type component. This component could derive by partial melting of the

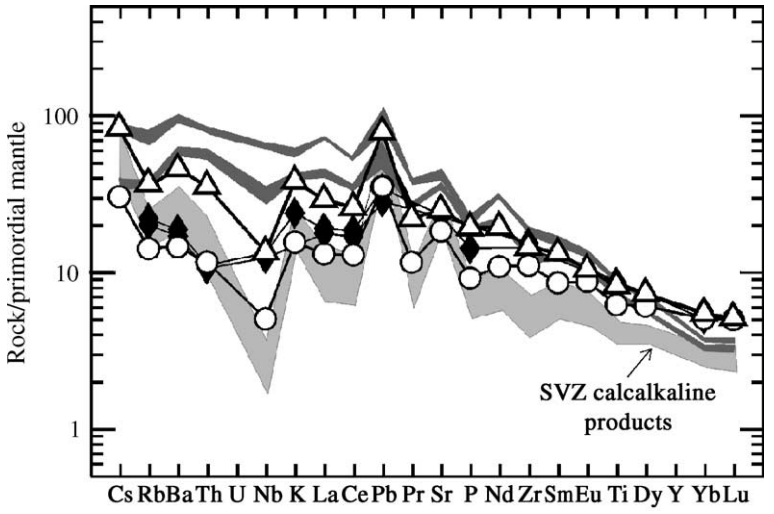

Fig. 9. Primitive mantle-normalised trace element diagrams (normalisation factors from Sun and Mc Donough, 1995) of selected basalts from the southernmost portion of the SVZ volcanic arc. Hudson (open triangles, this work), Río Ibanez (open circles, this work), Murta (full diamonds, Demant et al., 1998), Puyuhuapi (dark grey fields, González-Ferrán et al., 1996) and calc-alkaline volcanoes of the SVZ (light grey field, this work and D'Orazio et al., 2003 and references therein).

continental lithosphere due to the thermal input following the opening of the slab window. The Puyuhuapi basalts, having a clear intraplate signature, were explained with a partial melting processes at the base of the sub-continental lithosphere, as a response to the extensional tectonic stress along the LOF system (González-Ferrán et al., 1996). Alternatively, the within plate OIB-like component could be related to the vicinity of the slab window, which allowed the upflow of sub-slab asthenospheric mantle (e.g., Ramos and Kay, 1992; Gorring et al., 1997; D'Orazio et al., 2001).

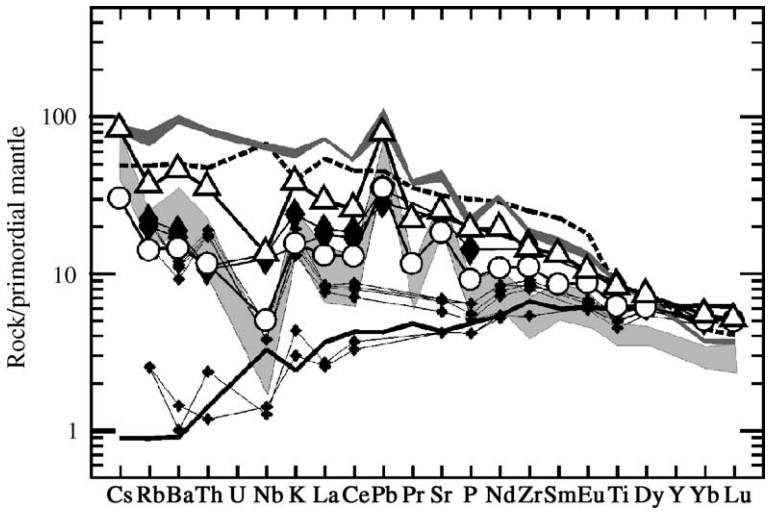

Fig. 10. Primitive mantle-normalised trace element diagrams (normalisation factors from Sun and Mc Donough, 1995) of Hudson and Río Ibanez basalts compared to the products of Patagonian volcanic centres cited in the discussion. Black crosses: Taitao Ridge basalts (Guivel et al., 1999), dashed line: OIB (Sun and Mc Donough, 1995), continuous line: N-MORB (Sun and Mc Donough, 1995), other symbols as in Fig. 9. The MC samples from this work plot in the calc-alkaline SVZ field and are not distinguished for clarity.

6.2. Differentiation processes

In the variation diagrams (Fig. 7a,b), RI basalts plot on the same trend of HV rocks, at the most primitive end, suggesting that RI and HV rocks may be parental and cogenetic. This is confirmed by their similar trace element patterns (Fig. 9) and by the similarity of some trace element ratios (Table 5). The HV basaltic magmas could derive from a primary magma originated from the same mantle source of RI through fractional crystallisation plus crustal assimilation processes occurred during storage in the crust. Least squares calculations, whose results are reported in Fig. 12a, show that HV mafic rocks may be derived from RI basalt through 16% fractional crystallisation of a mineral assemblage dominated by plagioclase, olivine and minor clinopyroxene, joined to assimilation of upper crust material with r in the range 0.1–0.3 (DePaolo, 1981). The results of the model (field in Fig. 12a) are in good agreement with the data. Crystal fractionation without crustal assimilation could not model the Rb, Ba and Th enrichment of HV with respect to RI. The involvement of upper crust contamination is also suggested by the higher $^{87}Sr/^{86}Sr$ and lower $^{143}Nd/^{144}Nd$ of HV basalts with respect to the monogenetic cones (i.e., Murta, Fig. 11d).

The compositional range of the HV rocks can be explained with a fractional crystallisation process, involving mainly plagioclase and pyroxene (Fig. 12b). Least squares geochemical modelling was carried out, showing that 31–42% crystal fractionation involving 72–82 vol.% plagioclase, 11–22 vol.% clinopyroxene and less than 7 vol.% Fe–Ti oxides allows generation of basaltic andesites from basalts. The most differentiated products, high-K dacites, may be generated by crystal fractionation dominated by orthopyroxene. The strong decrease of P_2O_5 in dacites indicates the participation of apatite, a common accessory, to the fractionating assemblage. The presence of weak Eu anomalies in the REE patterns of dacitic samples (Fig. 8b) suggests that fractionation of plagioclase occurs at an oxygen fugacity sufficient to have some Eu in the bivalent state, so that it can be slightly fractionated in respect to the other rare earths. The calculated values of oxygen fugacities (Table 3) are in agreement with the occurrence of a minor Eu anomaly, if compared with the experimental results of Wilke and Behrens (1999).

6.3. Tectonic control on magma composition, storage and ascent

In the southernmost sector of SVZ, the central volcanoes (Maca, Cay and Hudson) are roughly aligned along the N–S strike, following the general trend of Andean active volcanic arc, whereas the numerous small monogenetic cones are widespread in the area between 45° and 46°S (Fig. 2a). The main stratigraphical and topographical features and the historical records of central composite volcanoes indicate that they erupted frequently, with relatively high volumes of magmas and with a markedly different composition from basaltic andesites to dacites. The eruption of lava flows and pyroclastic products formed high edifices reaching 2000 to 2500 m elevations. This suggests that magma chambers within the crust were periodically supplied with magmas from the upper mantle. Although the Hudson centre did not build a typical stratovolcano-like

Table 5
Average values of selected trace element ratios in the products of Patagonian volcanic centres

	Chile Ridge, Taitao Ridge	Murta	Rio Ibanez	Hudson	Maca, Cay	Patagonian slab-window basalts	Average N-MORB	Average E-MORB	Average OIB
Ba/Nb	6–29	13.5–16	28.3	33–33.4	94–102	8–10	2.7	6.87	7.29
Ba/La	4–20	9.8–10	11.3	14–16	24–28	10–15	2.52	9.05	9.46
Th/Ta	0.9–4.1	1.54–1.58	3.7	3.8–4.9	9.1–10.2	1.2–1.7	0.91	1.28	1.48
La/Nb	0.8–2.1	1.4	1.9–2.5	2.1–2.4	3.6–3.9	0.6–0.8	1.07	0.76	0.77
Zr/Y	2.3–4.2	5	4.8	5.3–6.5	2.9–4.2	7–9	2.64	3.32	9.66
Ti/Y	225–296	348	314	354	304–339	650–730	271	273	356
Th/Yb	0.04–0.68	0.34–0.36	0.40	0.9–1.1	0.6–1	2–2.8	0.04	0.25	1.85

Data from this work, Klein and Karsten (1995), Demant et al. (1998) and Lagabrielle et al. (2000).

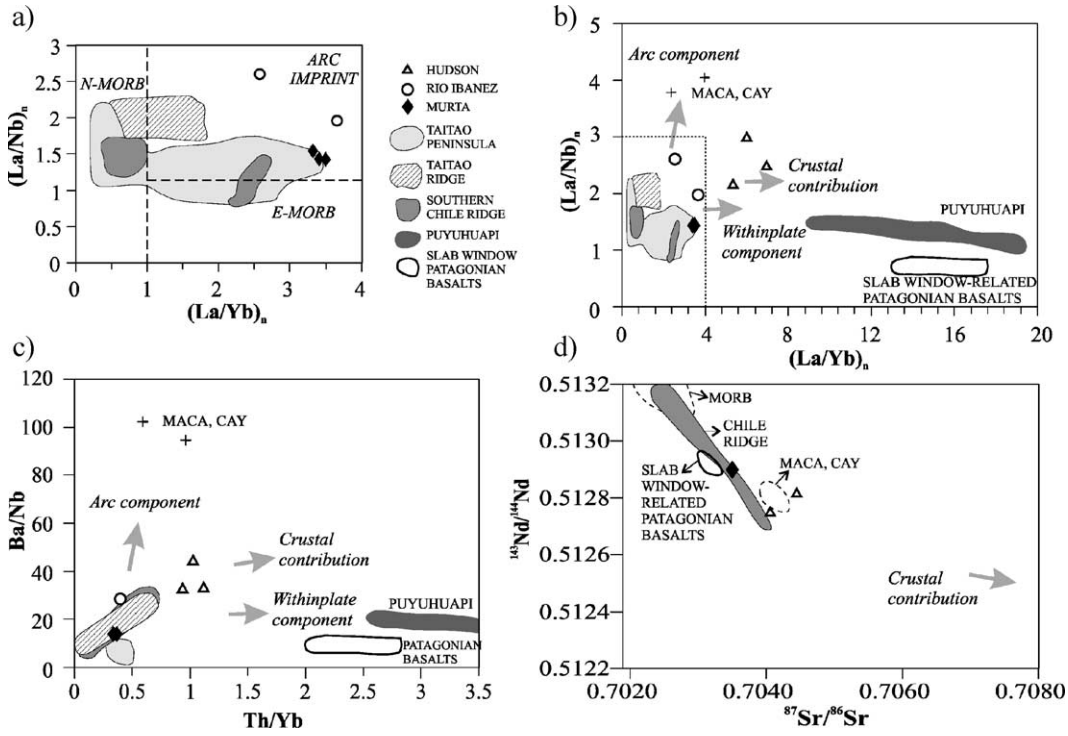

Fig. 11. (a) $(La/Yb)_N$ vs. $(La/Nb)_N$ diagram, showing the Río Ibanez and Murta basalts compared to the basalts of the Chile Ridge (Klein and Karsten, 1995), the Taitao Ridge and the Taitao Peninsula (Guivel et al., 1999). The dashed lines separate fields as in Guivel et al. (1999). Chondrite-normalisation factors from Sun and Mc Donough (1995). (b) $(La/Yb)_N$ vs. $(La/Nb)_N$ diagram and (c) Ba/Nb vs. Th/Yb diagram showing the Río Ibanez and Murta basalts compared to the volcanic products of the area (data sources as in Figs. 6 and 7; slab-window Patagonian basalts from D'Orazio et al., 2001; Gorring and Kay, 2001). (d) $^{143}Nd/^{144}Nd$ vs. $^{87}Sr/^{86}Sr$ diagram plotting the available data for Hudson (Lopez-Escobar et al., 1993) and Murta (Demant et al., 1998); fields are also shown for Maca and Cay (D'Orazio et al., 2003), Chile Ridge (Klein and Karsten, 1995) and slab-window Patagonian basalts (D'Orazio et al., 2001; Gorring and Kay, 2001).

edifice, it was active for at least 1 Ma (Orihashi et al., 2004) and produced several huge eruptions (up to the >18 km^3 tephra of the 6700 BP event, Naranjo and Stern, 1998), revealing the existence of a large volume, repeatedly fed magma chamber. On the contrary, the monogenetic centres, some of which are very close to the composite volcanoes, are characterised by short-lived strombolian activity that constructed cinder and spatter cones 200 to 300 m high and by small and fluid basaltic lava flows. The volume of products erupted by these centres is always small, ranging from about 4 and 7×10^6 m^3 based on our field data. These differences, linked to the fault systems controlling volcanism, are difficult to explain because detailed structural data are very limited in this Andean sector. However, it is presumable that, under the central composite volcanoes, the geological and tectonic conditions exist for the formation of tectonic traps where the magma may pond and differentiate. The magmas linked to the monogenetic cones, instead, erupt to the surface directly from the upper mantle without finding the geological conditions for ponding within the crust. Some hypothesis can be done for explaining these different dynamics of magma storage and ascent, taking into account the tectonic features of the area and correlating them with the distribution of the volcanic edifices.

The distribution of monogenetic volcanoes analysed with the Fry method (Fig. 2d) indicates that these centres are mainly aligned along NNE–SSW strike, that is parallel to the LOF system trend (Fig. 2a,b). This means that this structure has a lithospheric importance and a transtesional regime such to permit the magmas to reach rapidly to the surface. In this

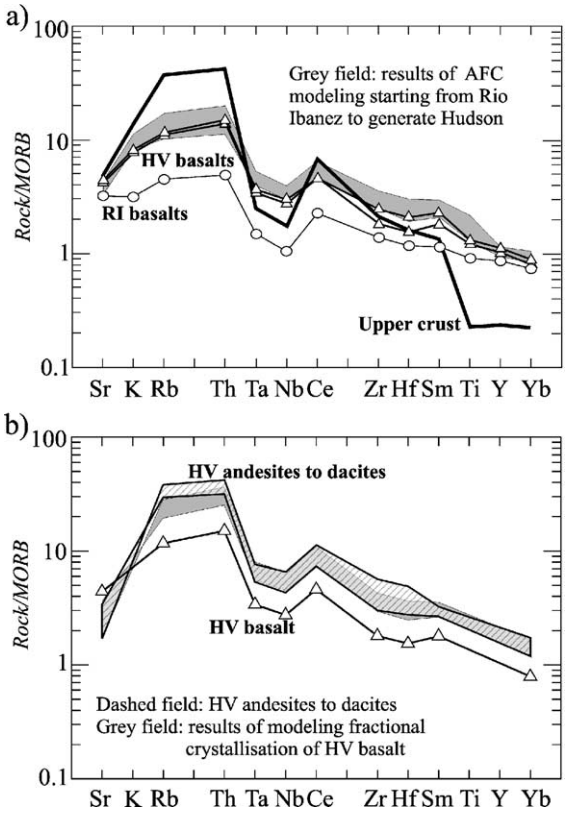

Fig. 12. MORB-normalised trace element diagrams (normalizing factors from Pearce, 1983) showing (a) the results of AFC modelling starting from the Río Ibanez basalt to obtain the Hudson basalt; fractionating phases: plagioclase, olivine, clinopyroxene; contaminant ($r = 0.1–0.3$): upper crust (Zindler and Hart, 1986); (b) the results of FC modelling starting from the HV basalt to obtain the HV differentiated products from andesites to dacites (see text for explanations).

sector, the LOF dextral system is characterised by two main branches and some conjugate faults with NE–SW strike connecting the two branches (Fig. 2a). These are transcurrent faults with an extensional component forming local pull-apart structures along which cavity-like magma chambers could form. Once these magma reservoirs have emplaced, they concentrate local tensile stress, which creates the conditions for a frequent rupture of the crustal segment above the chamber with consequent frequent eruptions constructing the large stratovolcanoes. The concentration of the local stress field near magma chambers could explain the repeated injection of magma from the mantle (Gudmudsson, 1998). The local extensional stress field related to the conjugate transversal fault systems (Fig. 2c) joined to the partial emptying of magma reservoir, probably played an important role also in the HV caldera formation.

The transcurrent tectonics, therefore, has a crucial importance in determining the geometry of the volcanic edifices including the HV caldera formation, the dynamics of magma ascent and storage and magma geochemical features. In some cases, the tectonics allowed the storage, evolution and mixing of magmas in the crust and the emplacement of large composite volcanoes (i.e., HV and MC), and in some other cases permitted brief strombolian eruptions of mafic magmas that maintained geochemical features of the mantle source without significant crustal input (i.e., Río Murta, Río Ibanez and Puyuhuapi).

6.4. Geodynamic implications

The currently accepted model for explaining the geodynamic evolution from Miocene up to the present in the southern segment of Andean Cordillera concerns the interaction of the spreading Chile Ridge with the South America continental margin. At present, the Chile Ridge–Trench collision (Chile Triple Junction) is located near the Taitao Peninsula at 46°12′S. The Chile Ridge segment which is presently subducting is oriented N20W and entered the Chile Trench about 0.3 Ma ago (Lagabrielle et al., 2000 and references herein). Two short ridge segments were previously subducted at about 6 and 3 Ma (Cande and Leslie, 1986, Fig. 1). Fig. 1 shows the schematic features of the Antarctic and Nazca Plates along the South America continent (Lagabrielle et al., 2000) with the continuation of the spreading ridge structures under the continental lithosphere. In agreement with this geometric model of the plates, the subducted segments of the Chile Ridge at about 6 and 3 Ma would be located close to HV and the surrounding monogenetic cones. The FZ Tres Montes (Fig. 1) would represent the northern border of the slab window. South of this FZ the volcanism and seismic activity cease. Several recent papers deal with the relationships between the magmatism emplaced on Taitao Peninsula and the interaction of Chile Ridge with the Chile Trench (Guivel et al., 1999; Lagabrielle et al., 2000 and references herein). These authors carried out a detailed study of the

geological and structural characteristics of the Taitao Peninsula and of the geochemical features of volcanic and intrusive products outcropping there. These authors explain the presence of adakitic magmas as derived by partial melting of subducted oceanic crust, and MORB type basalts as partial melting products of the depleted asthenosphere associated with the subduction of the Chile Ridge. The genesis of the felsic intrusive rocks is explained by anatexis of the continental crust for the high thermal gradients due to the subduction of the ridge segments. In this context, we attempt to explain the RI, Murta and HV geochemical characteristics starting from the general model proposed by these authors. Fig. 13 contains in (a) a cartoon of the geological setting of the South America continental margin between 45° and 47°S and in (b) the cross-sections at 45°, 46° and south of 47°. In this model, Murta, RI and HV magmas have the mantle source characteristics of the depleted asthenosphere under the subducted ridge. In this zone, fragments of subducted oceanic crust are still present and the mantle wedge is deeply modified by subduction-related components. The MORB-type primary magma is modified by altered oceanic crust and variably mixed with calc-alkaline magmas. The geochemical data indicate that a third magma component with OIB characteristics interacted with the above magma sources. The within-plate component could be derived by partial melting of sub-continental lithosphere following a process similar to that which generated the alkaline magmas erupted at the Puyuhuapi monogenetic centres. Alternatively, the OIB component could be linked to the lateral flow of asthenospheric mantle at the border of the slab window. South of 47°S, where the slab windows opened 6 to 14 Ma ago, the unmodified asthenospheric mantle has completely replaced the mantle modified by subduction and the erupted magmas show a clear OIB signature (Gorring and Kay, 2001; D'Orazio et al., 2001).

7. Conclusions

The HV, RI and Rio Murta are the volcanic manifestations located at the southernmost end of the SVZ and close to the impact zone between the Chile Ridge and the Chile Trench. The study of the products erupted by these volcanoes is therefore of great importance to understand volcanism in a ridge–trench collision geodynamic setting such as the South American margin between 45° and 47°S. The geo-

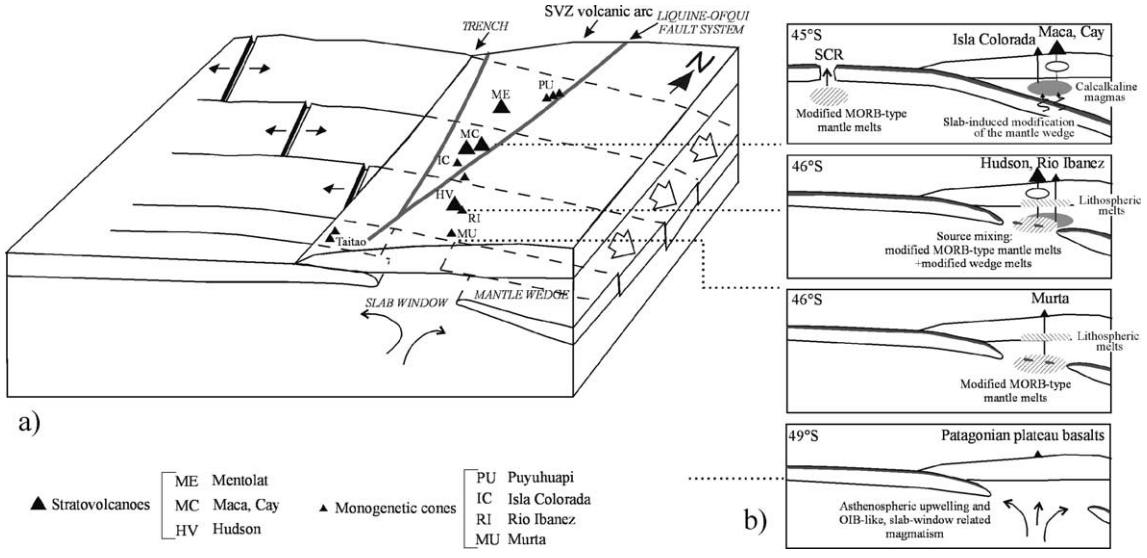

Fig. 13. Block diagram (a) sketching the position of the volcanoes of the southernmost SVZ in respect to the ridge–trench collision and to the consequent opening of the slab window. On the right (b), cross-sections are drawn illustrating the different conditions in which magma generation occurs from 45°S southwards.

logical, volcanological and geochemical data presented have permitted to us to make the following conclusive remarks:

1) The HV is characterised by a quasi-circular caldera set in the Patagonian Batholith. Field evidence and rough calculations of the volumes of the caldera depression and of pre-caldera lavas, compared to previous volume estimations of recent and prehistoric pyroclastic deposits, suggest that the caldera formed incrementally and most probably in relatively recent times. The local extensional stress field, related to the conjugate transversal fault systems linked to the LOFS, probably played a relevant role in the caldera formation. Glacial erosion concurred to the present morphology.
2) The zones of interaction between two main tectonic trends (NNE–SSW and NE–SW) are responsible for ponding of magmas in relatively shallow levels of the continental crust. Magma chambers were replenished by mantle-derived magmas, which were contaminated with crustal materials and mixed with resident differentiated felsic magmas. Repeated effusive and explosive eruptions formed large composite volcanoes.
3) The transtensive regime of LOF system permitted the ascent of relatively primitive magmas which gave rise to monogenetic cinder and spatter cones surrounding the HV. Due to their primitive nature, these lavas give important clues on the geochemical characteristics of the mantle source(s), which are responsible also for the HV magmatic activity. Major and trace element characteristics of basalts of the RI and Murta cones is quite similar to basalts dredged on the Chile and Taitao Ridges and to those outcropping on the Taitao peninsula. Based on the entire geochemical database, we have recognised three main magma components in the RI and Murta lavas: (a) a MORB like component, modified by altered oceanic crust and sediments, analogous to the Chile and Taitao Ridge basalts; (b) an arc component, linked to interaction of MORB-like magmas with pockets of fluid/melt modified mantle stored at the base of the lithosphere; (c) an intraplate component linked to either the partial melting of continental lithosphere along the LOF system or to lateral asthenospheric flow through the slab window to the south.
4) The individuation of the different components active in the magma sources at the border of a slab window in south Patagonia margin led to formulate a model for magma generation in such a complex geodynamical setting.

Acknowledgements

The authors are indebted to Engineer Robert Biehl, General Manager of the NORANDA-ALUMISA project, for the kind permission to use the volcanic rocks and geological data from Hudson Volcano, under the Centro de Estudios Volcanológicos de Santiago, Chile. M. D'Orazio is thanked for the technical assistance during the ICP-MS trace element determinations and for the discussions on Patagonian magmatism. F. Olmi is acknowledged for technical help with the electron microprobe. The authors are also grateful to M. Bertoli and M. Tamponi for carrying out XRF and LOI determinations, to F. Colarieti for the preparation of polished rock sections and to M. Menichini for the XRF analysis.

The manuscript was significantly improved by the detailed and thoughtful comments of M.L. Gorring. The authors also thank an anonymous referee for his/her appreciated suggestions.

The paper was partly supported by PNRA funds and by Pisa (fondi d'Ateneo) funds to R. Mazzuoli.

References

Barrientos, S.E., Plafker, G., 1992. Post seismic coastal uplift in Southern Chile. Geophys. Res. Lett. 19 (7), 701–704.

Bence, A.E., Albee, 1968. Empirical correction factors for the electron microanalysis of silicates and oxides. J. Geol. 76, 382–403.

Branney, M.J., Gilbert, J.S., 1996. Ice-melt collapse pits and associated features in the 1991 lahar deposits of the Volcan Hudson, Chile: criteria to distinguish eruption-induced glaciar melt. Bull. Volcanol. 57, 293–302.

Cande, S.C., Leslie, R.B., 1986. Late Cenozoic tectonics of the southern Chile Trench. J. Geophys. Res. 91 (B1), 471–496.

Cande, S.C., Leslie, R.B., 1987. Interaction between the Chile Ridge and Chile Trench: geophysical and geothermal evidence. J. Geophys. Res. 92 (B1), 495–520.

Cembrano, J., Schermer, E., Lavenu, A., Hervé, F., Barrientos, S., McClelland, B., Arancibia, G., 1996a. Nature and timing of Cenozoic intra-arc deformation, Southern Chile. Third International Symposium on Andean Geology, St. Malo, France, pp. 311–314.

Cembrano, J., Hervé, F., Lavenu, A., 1996b. The Liquiñe Ofqui fault zone: a long-lived intra-arc fault system in southern Chile. Tectonophysics 259, 55–66.

Demant, A., Hervé, F., Pankhurst, R.J., Magnette, B., 1994. Alkaline and calc-alkaline Holocene basalt from minor volcanic centres in the Andes of Aisén, southern Chile. VII Congreso Geológico Chileno, Actas, vol. 2, pp. 1326–1330.

Demant, A., Belmar, M., Hervé, F., Pankhurst, R.J., Suarez, M., 1998. Petrologie et geochimie des basaltes de Murta: une eruption sousglaciaire dans les Andes patagoniennes (468 lat. S.), Chili. Relation avec la subduction de la ride du Chili. C. R. Acad. Sci., Paris 327, 795–801.

DePaolo, D.J., 1981. Trace element and isotopic effects of combined wall-rock assimilation and fractional crystallization. Earth Planet. Sci. Lett. 53, 189–202.

Deruelle, B., Bourgois, 1993. Sur la dernière éruption du volcan Hudson (sud Chili, aout 1991). C. R. Acad. Sci., Paris 316, 1399–1405.

D'Orazio, M., Agostini, S., Mazzarini, F., Innocenti, F., Manetti, P., Haller, M.J., Lahsen, A., 2001. The Pali Aike volcanic field, Patagonia: slab-window magmatism near the tip of South America. Tectonophysics 321, 407–427.

D'Orazio, M., Innocenti, F., Manetti, P., Tamponi, M., Tonarini, S., González-Ferrán, O., Lahsen, A., 2003. The Quaternary calc-alkaline volcanism of the Patagonian Andes close to the Chile Triple Junction: geochemistry and petrogenesis of volcanic rocks from Cay and Maca Volcanoes (~ 45°S, Chile). J. South Am. Earth Sci. 16, 219–242.

Forsythe, R., Nelson, E., 1985. Geological manifestations of ridge collision: evidence from the Golfo de Penas, Taitao Basin, southern Chile. Tectonics 4, 477–495.

Forsythe, R., Nelson, E., Carr, M., Kaeding, M., Hervé, M., Mpodozis, C., Soffia, J.M., Harambour, S., 1986. Pliocene near-trench magmatism in southern Chile: a possible manifestation of ridge collision. Geology 14, 23–27.

Franzini, M., Leoni, L., Saitta, M., 1975. Revisione di una metodologia analitica per fluorescenza X, basata sulla correzione complete degli effetti di matrice. Soc. It. Min. Petr. 31 (2), 365–378.

Futa, K., Stern, C.R., 1988. Sr and Nd isotopic and trace element composition of Quaternary volcanic centers of southern Andes. Earth Planet. Sci. Lett. 88, 253–263.

González-Ferrán, O., Innocenti, F., Lahsen, A., Manetti, P., Mazzuoli, R., Omarini, R., Tamponi, M., 1996. Alkali basalt volcanism along a subduction related magmatic arc: the case of Puyuhuapi Quaternary volcanic line, southern Andes (44°20′S). XIII Congreso Geológico Argentino y III Congreso de Exploración de Hidrocarburos, Actas, vol. III, pp. 549–565.

Gorring, M.L., Kay, S.M., 2001. Mantle sources and processes of Neogene slab window magmas from southern Patagonia, Argentina. J. Petrol. 42, 1067–1094.

Gorring, M.L., Kay, S.M., Zeitler, P., Ramos, V., Rubiolo, D., Fernandez, M., Panza, J.L., 1997. Neogene Patagonian Plateau lavas: continental magmas associated with ridge collision at the Chile Triple Junction. Tectonics 16, 1–17.

Gudmudsson, A., 1998. Magma chambers modeled as cavities explain the formation of rift zone central volcanoes and their eruption and intrusion statistics. J. Geophys. Res., B 103 (4), 7401–7412.

Guivel, C., Lagabrielle, Y., Bourgois, J., Maury, R.C., Fourcade, S., Martin, H., Arnaud, N., 1999. New geochemical constraints for the origin of ridge-subduction-related plutonic and volcanic suites from the Chile Triple Junction (Taitao Peninsula and Site 862, LEG ODP141 on the Taitao Ridge). Tectonophysics 311, 83–111.

Herron, E.M., Cande, S.C., Hall, B.R., 1981. An active spreading center collides with a subduction zone, a geophysical survey of the Chile Margin Triple Junction. Mem. Geol. Soc. Amer. 154, 683–701.

Hervé, F., 1984. La zona de falla de Liquiñe-Ofqui en Liquiñe. Comunicaciones 34, 101–105.

Hervé, F., Pankhurst, R.J., Drake, R., Beck, M.E., 1993. Pillow metabasalts in a mid-Tertiary extensional basin adjacent to the Liquiñe-Ofqui fault zone: the Isla Magdalena area, Aisén, Chile. J. South Am. Earth Sci. 8, 33–46.

Irvine, T.N., Baragaar, 1971. A guide to the chemical classification of the common volcanic rocks. Can. J. Earth Sci. 8 (5), 523–548.

Klein, E.M., Karsten, J.L., 1995. Ocean-ridge basalts with convergent margin geochemical affinities from the Chile Ridge. Nature 374, 52–57.

Lagabrielle, Y., Guivel, C., Maury, R.C., Bourgois, J., Fourcade, S., Martin, H., 2000. Magmatic-tectonic events of high thermal regime at the site of active ridge subduction: the Chile Triple Junction model. Tectonophysics 326, 255–268.

Lahsen, A., Gonzalez-Ferran, O., Innocenti, F., Manetti, P., Mazzuoli, R., Omarini, R., Tamponi, M., 1997. New occurrence of orogenic volcanism along Liquide-Ofqui fault system: the Rio Pescado volcanic centers, southern Andes (45°30′S, 73°04′W), Chile. VIII Congreso Geologico Chileno, Actas, vol. I, pp. 108–112.

Lopez-Escobar, L., Kilian, R., Kempton, P., Tagiri, M., 1993. Petrography and geochemistry of Quaternary rocks from the southern volcanic zone of the Andes, between 41°30′ and 46°00′S, Chile. Rev. Geol. Chile 20, 33–55.

Naranjo, J.A., Stern, C.R., 1998. Holocene explosive activity of Hudson Volcano, southern Andes. Bull. Volcanol. 59, 291–306.

Naranjo, J.A., Moreno, H., Banks, N., 1993. La erupción del Volcán Hudson en 1991(46° S), Región XI, Aisén, Chile Bol., vol. 44. Servicio Nacional de Geología y Minería, Chile.

Nelson, E., Forsythe, R., Arit, I., 1994. Ridge collision tectonics in terrane development. J. South Am. Earth Sci. 7, 271–278.

Orihashi, Y., Naranjo, J.A., Motoki, A., Sumino, H., Hirata, D., Anma, R., Nagao, K., 2004. Quaternary volcanic activity of Hudson and Lautaro Volcanoes, Chilean Patagonia: new constraints from K–Ar ages. Rev. Geol. Chile 31, 207–224.

Pankhurst, R.J., Hervé, F., Rapela, C.R., 1994. Sm–Nd evidence for the Grenvillian provenance of the metasedimentary basement of

southern Chile and west Antarctica. Acta VII Congr. Geol. Chil. Conception, Chile, pp. 1414–1418.

Pearce, J.A., 1983. The role of sub-continental lithosphere in magma genesis at destructive plate margins. In: Hawkesworth, C.S., Norry, M.J. (Eds.), Continental basalts and mantle xenoliths, pp. 230–249.

Ramos, V.A., Kay, S.M., 1992. Southern Patagonian Plateau basalts and deformation: back-arc testimony of ridge collision. Tectonophysics 205, 261–282.

Serv. Nac. Geol. Min., 1982. Mapa Geológico de Chile, Escala 1:1.000.000. Hoja No. 5, entre los 43°30′–49°3′S. Publicado por el Instituto Geográfico Militar, Chile.

Sisson, T.W., Grove, T.L., 1993. Temperatures and H_2O contents of low-MgO high-alumina basalts. Contrib. Mineral. Petrol. 113, 167–184.

Spencer, K., Lindsley, D.H., 1981. A solution model for coexisting iron–titanium oxides. Am. Mineral. 66, 1189–1201.

Stern, C.R., 1991a. Role of subduction erosion in the generation of Andean magmas. Geology 19, 78–81.

Stern, C.R., 1991b. Mid-Holocene Tephra on Tierra del Fuego (54° S) derived from the Hudson Volcano: evidence for a large explosive eruption. Rev. Geol. Chile 18, 139–146.

Stern, C.R., Kilian, R., 1996. Role of the subducted slab, mantle wedge, and continental crust in the generation of adakites from the Andean Austral Volcanic Zone. Contrib. Mineral. Petrol. 123, 263–281.

Stern, C., Frey, F., Futa, K., Zartman, R., Peng, Z., Kyser, T., 1990. Trace-element and Sr, Nd, Pb, and O isotopic composition of Pliocene and Quaternary alkali basalts of the Patagonian Plateau lavas of southernmost South America. Contrib. Mineral. Petrol. 104, 294–308.

Sun, S.S., Mc Donough, W.F., 1995. The composition of the earth. Chem. Geol. 120, 223–253.

Vaggelli, G., Olmi, F., Conticelli, S., 1999. Quantitative electron microprobe analysis of reference silicate mineral and glass samples. Acta Vulcanol. 11, 297–304.

Vearncombe, J., Vearncombe, S., 1999. The spatial distribution of mineralization: applications of Fry analysis. Econ. Geol. 94, 475–486.

Wilke, M., Behrens, H., 1999. The dependence of partitioning of iron and europium between plagioclase and hydrous tonalitic melt on oxygen fugacity. Contrib. Mineral. Petrol. 137, 102–114.

Zindler, A., Hart, S.R., 1986. Chemical geodynamics. Annu. Rev. Earth Planet. Sci. 14, 493–571.